# REDOX-RESPONSIVE COLLOIDOSOMES VIA SUPRAMOLECULAR CHEMISTRY

by

Hasan Can Helvacı

B.S., Chemistry, Bogazici University, 2013

Submitted to the Institute for Graduate Studies in
Science and Engineering in partial fulfillment of
the requirements for the degree of
Master of Science

Graduate Program in Chemistry
Boğaziçi University

2015

*Dedicated to my family and my beloved Özge İnan*

# ACKNOWLEDGEMENTS

I would like to state my gratefulness to my supervisor Assoc. Prof. Amitav Sanyal to give me the opportunity to work in his research group. I gained numerous experience during four years in Sanyal lab as a master and an undergraduate student. Working in different projects has provided me to learn new concepts and gain an understanding of problem solving.

I wish to express my thanks to Assoc. Prof. Rana Sanyal for her scientific advices and her helpful discussions regarding all my research in this laboratory.

I wish to express my thanks to Prof. Assoc. Prof. Şenol Mutlu for his careful and constructive review of the final manuscript.

I am so glad to work with enthusiastic and hardworking friends. I wish to express my great thanks to Tuğçe Nihal Gevrek for her support and helpfulness during my study. Also, I want to thank Mehmet Arslan for his guidance on my thesis. I would like to thank Filiz Emlik Çalık, Burcu Sümer, Özgül Gök and Merve Karaçivi for their patience and helpfulness for my synthesis and analysis.

I would like to thank my labmates Sesil Genç, Hazal İpek, Buğra Aktan, Duygu Aydın, Özlem Kalaoğlu Altan, Laura Chambre, Gizem Yeter Baş, İsmail Altınbaşak, Azize Kıraç, Büşra Karagöz, Bianca Golba, Ahmet Yeşilçimen and Evrim Arslan for their friendship and endless support. I would also thank all my friends and the members of the faculty in Chemistry Department.

This work was supported by The Scientific and Technological Research Council of Turkey (TÜBİTAK) (113Z235).

# ABSTRACT

## REDOX-RESPONSIVE MICROCAPSULE SYSTEMS VIA SUPRAMOLECULAR CHEMISTRY

In supramolecular chemistry, molecules can be assembled together through non-covalent interactions without management from an outside source in order to form well-organized structures such as micelles, microspheres, interface (membrane) or colloidal microcapsules. This thesis focused on formation and stabilization of self-assembled microcapsules by using host-guest interaction, encapsulation biomolecules into these microcapsules and controlled released of them after the microcapsules exposed to reducing agent. In this study, β-cyclodextrin functionalized gold nanoparticles were used as host molecules and bis-adamantane containing linker molecules and adamantine functionalized iron oxide nanoparticles were used as guest molecules. Due to strong interaction between adamantine and β-cyclodextrin molecules, stable microcapsules were obtained as a result of cross-linking host and guest molecules at water-organic interfaces of emulsions. Then the disassembly of microcapsules was analyzed after exposure to reducing agent. Resulting microcapsules were characterized using a variety of techniques such as optical microscopy, fluorescence microscopy, transmission electron microscopy (TEM) and scanning electron microscopy (SEM).

# ÖZET

## SUPRAMOLEKÜLER KİMYA YOLUYLA KURULAN REDOKS-DUYARLI MİKROKAPSÜLLER

Supramoleküler kimyada, dışarıdan bir müdahale olmadan moleküller, aralarındaki kovalent olmayan belirli etkileşimler sayesinde bir araya gelerek daha organize, işlevsel malzemeleri oluşturabilirler. Misel, mikroküre, membran ya da koloidal mikrokapsüller gibi değişik yapılar bu malzemelere örnek olarak verilebilir. Bu tezde genel olarak, konuk-konak kompleksleşmesi metoduyla kovalent bağlı olmayan su bazlı ve tersinir mikrokapsüllerin eldesini, biyomolekül enkapsülasyonunu ve bu malzemelerin indirgeyen maddeler ile bozunarak biyomolekül salımının gerçekleştirilmesini hedeflemiştir. Bu çalışmada, β-siklodekstrin kaplı altın nanoparçacıklar konak molekül olarak, adamantan grubu olan bağlayıcı moleküller ve adamantan kaplı demir oksit nanoparçacıklar konuk molekül olarak sentezlenmiştir. Siklodekstrin molekülü ve adamantan moleküllü arasındaki etkileşimi kullanarak, konuk ve konak yapıların su/organik-solvent emülsiyonu ara yüzeyinde çaprazlanmalarıyla birlikte kararlı mikrokapsüller elde edilmiştir. Ayrıca elde edilen mikrokapsullerin, indirgeyen maddelere maruz bırakıldıklarındaki bozulmaları incelenmiştir. Elde edilen mikrokapsüller optik mikroskopi, flüorsan mikroskopi, transmisyon elektron mikroskopi (TEM) ve taramalı elektron mikroskopi teknikleriyle gözlemlenmiştir.

# TABLE OF CONTENTS

# LIST OF FIGURES

# LIST OF TABLES

# LIST OF ACRONYMS / ABBREVIATIONS

| | |
|---|---|
| AD-$Fe_3O_4$ | Non-Redox Responsive Adamantane Functionalized Iron Oxide Nanoparticles |
| AD-N-O-N-AD | Non-Redox Responsive Bisadamantane Containing Linker Molecule |
| AD-N-SS-N-AD | Redox Responsive Bisadamantane Containing Linker Molecule |
| AD-SS-$Fe_3O_4$ | Redox Responsive Adamantane Functionalized Iron Oxide Nanoparticles |
| $CDCl_3$ | Deuterated Chloroform |
| $CH_3CN$ | Acetonitrile |
| $CH_3ONa$ | Sodium Methoxide |
| DCM | Dichloromethane |
| DCPD | Dicyclopetadiene |
| DLS | Dynamic Light Scattering |
| DMAP | 4-Dimethylaminopyridine |
| DMF | Dimethylformamide |
| DMSO | Dimethyl Sulfoxide |
| DTT | Dithiothreitol |
| EDCI | 1-Ethyl-3-(3-dimethylaminopropyl) Carbodiimide |
| GSH | Glutathione |
| $HAuCl_4$ | Hydrogen Tetrachloroaurate (III) Hydrate |
| HCl | Hydrochloric Acid |
| $I_2$ | Iodine |
| $KHSO_4$ | Potassium Bisulfate |
| MeOH | Methanol |
| $NaBH_4$ | Sodium Borohydride |
| $NaHCO_3$ | Sodium Bicarbonate |
| NaOH | Sodium Hydroxide |
| $Na_2SO_4$ | Sodium Sulphate |

| | |
|---|---|
| NMR | Nuclear Magnetic Resonance |
| NPs | Nanoparticles |
| SEM | Scanning Electron Microscopy |
| TEM | Transmission Electron Microscopy |
| TFA | Trifluoroacetic Acid |
| THF | Tetrahydrofuran |

# 1. INTRODUCTION

## 1.1. Supramolecular Chemistry

Supramolecular chemistry focuses on chemical systems composed of various assembled molecular subunits or components. The forces responsible for forming this system may vary from weak (intramolecular forces, electrostatic or hydrogen bonding) to strong covalent bonding [1]. While traditional chemistry focuses on the covalent bond, supramolecular chemistry benefits from the weaker and reversible non-covalent interactions between molecules. These forces include hydrogen bonding, metal coordination, hydrophobic forces, van der Waals forces, pi-pi interactions and electrostatic effect whose strengths shown in the Table 1.1. [2]. Besides, crucial concepts that have been demonstrated by supramolecular chemistry include molecular self-assembly, folding induced by molecular recognition and host-guest chemistry [3].

Table 1.1. Strength of non-covalent interactions.

| **Type of Non-Covalent Interactions** | **Strength (kJ mol$^{-1}$)** |
|---|---|
| Hydrogen Bond | 2-30 |
| Metal Ligand | 0-400 |
| Hydrophobic | <10 |
| Van Der Waals Forces | 0.1-1 |
| Pi-Pi Interactions | 0-10 |
| Electrostatic Effect | 1-20 |

### 1.1.1. Molecular Self-Assembly

Molecular self-assembly is the construction of systems beyond a single molecule which occurs spontaneously. Without guidance or management from an outside source, molecules can be assembled together through non-covalent interactions. In nature, self-assembly is present in many biological systems in order to obtain highly ordered structures

such as the phospholipid bilayer cell membrane and liposomal constructs. Scientist have also developed many materials such as micelles, microspheres, vesicles, self-assembled monolayers or colloidal microcapsules inspired by self-assembled structures in nature [4].

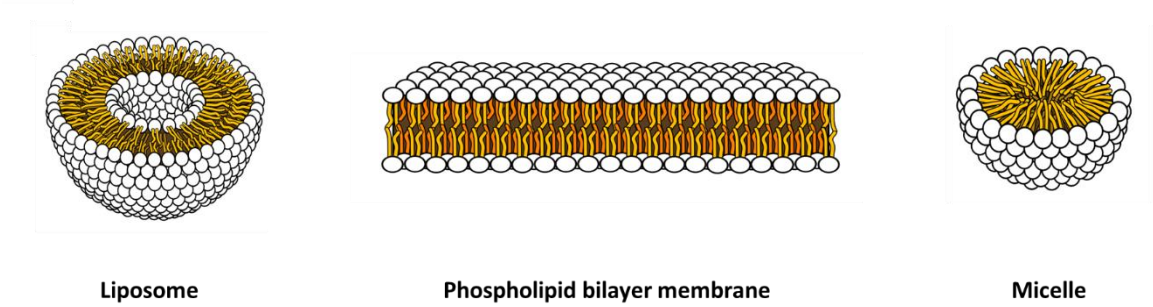


Figure 1.1. Examples of self-assembled structures in nature and science.

### 1.1.2. Molecular Recognition or Host-Guest Chemistry

Molecular recognition derives from the specific binding affinity between a guest molecule and its complementary host molecule to form a reversible host-guest complex (Figure 1.2.). In the host-guest chemistry, molecules are able to recognize each other using non-covalent interactions such as hydrogen bonding, van der Waals forces, pi-pi interactions, hydrophobic forces, electrostatic effects and metal coordination. As a result, host and guest molecules can be used as building blocks to fabricate larger well-defined structure using supramolecular chemistry [2].

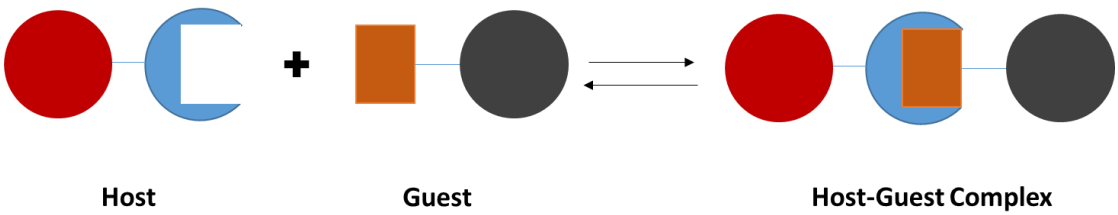


Figure 1.2. Host-guest interaction to form self-assembled complex.

### 1.1.3. Building Blocks of Supramolecular Chemistry

In supramolecular system, functional building blocks are utilized to build up larger functional architectures. These building blocks can be divided in various subgroups in terms of their properties, which is shown in Table 1.2. and blocks with the desired properties can be chosen to fabricate larger structures[5].

Table 1.2. Building blocks of supramolecular chemistry.

| **Type of building block** | **Examples** |
|---|---|
| Synthetic Recognition Motifs | Crown ether, Porphyrins |
| Macrocycles | Cyclodextrins, Calixarenes |
| Structural Units | Nanoparticles, Dendrimers, Adamantane |
| Photo-/electro-chemically active units | Azobenzenes, Fullerenes |
| Biologically-derived units | DNA, Biotin, Enzymes |

1.1.3.1. Cyclodextrins. In supramolecular chemistry, host-guest interaction is mostly used for the interaction between building blocks. Among all potential hosts, cyclodextrins seems to be the most attractive ones because they are readily available water-soluble semi-natural products. They are produced from starch by using a simple enzymatic conversion process. Furthermore, they are produced in large amount by environmentally friendly technology and their cost is relatively low. Thanks to their inclusion complex forming ability, they are widely utilized in many industrial products, technologies, and analytical methods [6].

Typical cyclodextrins are α, β, and γ cyclodextrins which have 6, 7 and 8 repeating glucopyranoside units respectively (Figure 1.3a). In three dimension, cyclodextrins appear like a conical cylinder with large and small openings where primary and secondary hydroxyl group are located, respectively. Due to this hydroxyl group arrangement of cyclodextrin, the interior side of it displays less hydrophilic feature than the outside; therefore, inner cavity of cyclodextrins are able to host other hydrophobic ‘guest’ molecules. Each type of cyclodextrin has different inner volume (Figure 1.3b); consequently, the size of guest molecule is crucial for forming appropriate inclusion complex. For example, adamantane molecule is a perfect candidate as a guest molecule for β-cyclodextrin.

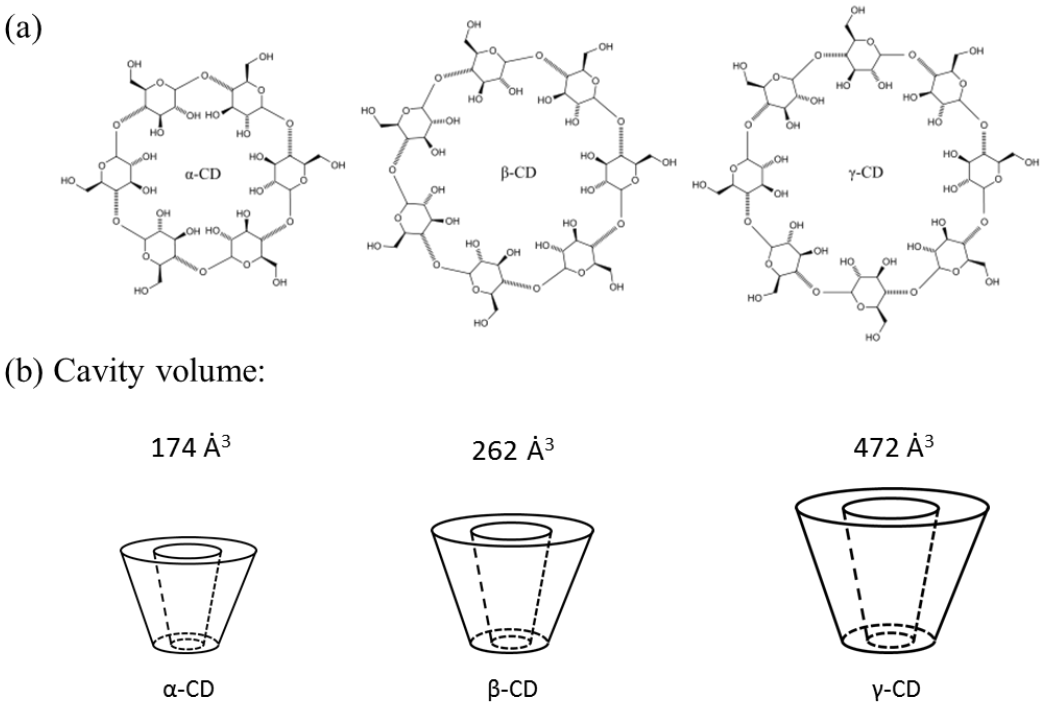


Figure 1.3. (a) Chemical structure of α, β, and γ cyclodextrins[7], (b) approximate cavitiy volume of α, β, and γ cyclodextrins.

1.1.3.2. Adamantane. One of the most common guest molecules for β-cyclodextrin is adamantane due to presence of strong interaction between each other (association constant is greater than $10^4$ $M^{-1}$). Adamantane molecule which is the simplest diamonded consists of 4 connected cyclohexane ring with a formula $C_{10}H_{16}$. Due to its apolar structure, adamantane molecule is soluble in organic solvents [8].

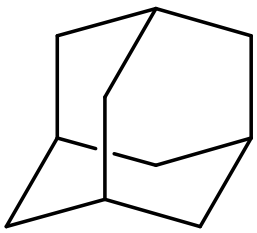

Figure 1.4. Chemical structure of adamantane molecule.

## 1.2. Colloidosomes or Microcapsules

Colloidosomes are selectively permeable capsules composed of colloidal particles, as originally defined by Dinsmore in 2002 [9]. After that, interest on this area has significantly increased due to their small size, high surface area, large inner volume and stable membrane properties. Furthermore, it is oftentimes possible to dry colloidosomes without the collapse by reinforcing the interaction between particles [9]. Due to these properties of colloidosomes, they have been applied as drug delivery vehicles, micro reactors, and catalyst supports and encapsulants [10].

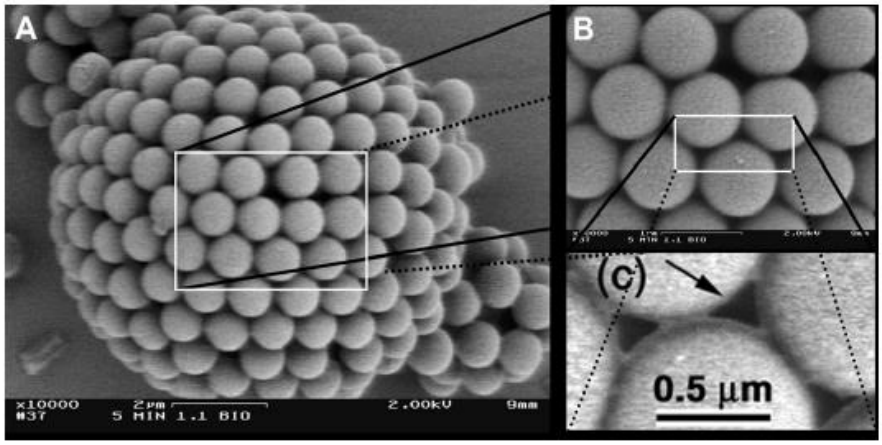


Figure 1.5. Scanning electron microscope image of a dried colloidosome.

There are various types of nano- and microcapsules recently developed such as liposomes [11], polymerosomes [12] and polyelectrolyte capsules [13] and they have a high potential to use for drug delivery, gene delivery and cancer therapy and other medical applications [14]. Mainly, there are two common ways to fabricate microcapsules. One of which is to use the self-assembly of lipids and/or polymers in order to form stable and well defined multifunctional microcapsules[12]. The other way is to stabilize emulsions via self-assembly of colloidal micro/nanoparticles at liquid-liquid interface [15]. Main advantage of the second approach is to benefit from properties of the nanoparticles such as their electric and optical features. For that purpose, gold and iron oxide nanoparticle can be the best candidate to serve as a functional building block for fabricating microcapsules, since gold nanoparticles display electronic and optical properties and iron oxide nanoparticles have

magnetic features. Additionally, by adjusting preparation conditions and the choice of colloids, physical properties of colloidal microcapsules such as permeability, mechanical strength, and biocompatibility can be controlled[16].

### 1.2.1. Building Blocks for Colloidal Microcapsules

1.2.1.1. Gold Nanoparticles. Au NPs have attracted huge scientific and technological interest due to their ease of synthesis, chemical stability, and unique optical-electronic properties [17]. They have been used in high technology applications such as sensory probes[18], therapeutic agent[19], drug delivery[20] in biology and medical application.

Two common methods used to synthesize stable gold nanoparticles. One of which is "citrate reduction" used by Turkevitch[21] . $HAuCl_4$ is reduced by trisodium 9 citrate in aqueous media. Besides, $HAuCl_4$ can be also reduced by $NaBH_4$ in order to obtain thiol stabilized Au NPs, which is called Brust-Schiffrin method (Figure 1.6.) [22].

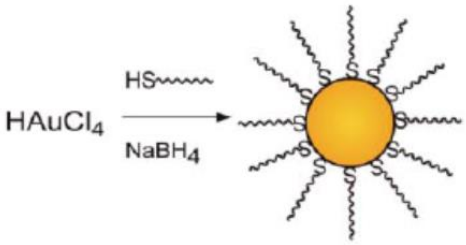


Figure 1.6. Synthesis of Au NPs via Brust-Schiffrin method[23].

Au NPs display optical and electronic properties which are tunable by adjusting their size, shape and surface chemistry because gold nanoparticles interactions which is strongly related to their environment, size and physical dimension[21].

Gold nanoparticles can display Surface Plasmon Resonance (SPR) in the visible light[24] which means that a certain portion of visible light will be absorbed, while the other portion will be reflected. The reflected portion will gain matter a certain color. For small

(~30nm) monodisperse gold nanoparticles the surface plasmon resonance phenomona causes an absorption of light in the blue-green portion of the spectrum (~450 nm) while red light (~700 nm) is reflected, which gives a rich red color. As particle size increases, the wavelength of surface plasmon resonance related absorption shifts to longer, redder wavelengths. Red light is then absorbed, and blue light is reflected, which yields solutions with a pale blue or purple color (Figure 1.7.).

Figure 1.7. Colors of various sized monodispersed gold nanoparticles [25].

As particle size continues to increase toward the bulk limit, surface plasmon resonance wavelengths move into the IR portion of the spectrum and most visible wavelengths are reflected, giving the nanoparticles clear or translucent color. The surface plasmon resonance can be tuned by varying the size or shape of the nanoparticles, leading to particles with tailored optical properties for different applications [25].

1.2.1.2. Iron Oxide Nanoparticles. Iron oxide nanoparticles (NPs) have attracted extensive interest due to their supramagnetic properties and their potential applications in hyperthermia [26], drug delivery [27], magnetic resonance imaging (MRI) contrast agent [28] and magnetic cell labeling [29]. The properties of nanoparticles are strongly dependent on the dimension of them; therefore, different procedures have been developed in order to produce and highly monodisperse NPs [28]. The important ones are thermal decomposition, co-precipitaion and microemulsion [30].

### 1.2.2. Pickering Emulsions

Emulsion can be stabilized by solid nanoparticles which locate onto the interface between two phases. This process was reported for the first time by Ramsden in 1903 [31]. However, it was called as Pickering emulsions after the article published by Pickering in 1907[32]. Since then, this field has not drawn significant attention until 1990. After Velev demonstrated its potential on microencapsulation and the development of novel colloid material, Pickering emulsions regained new interest[33]. After that, Weitz [34,35] and Bon[36,37] and their coworkers displayed that capsules from Pickering emulsions can be synthesized with a precise control of size, permeability and mechanical properties (Figure 1.8.).

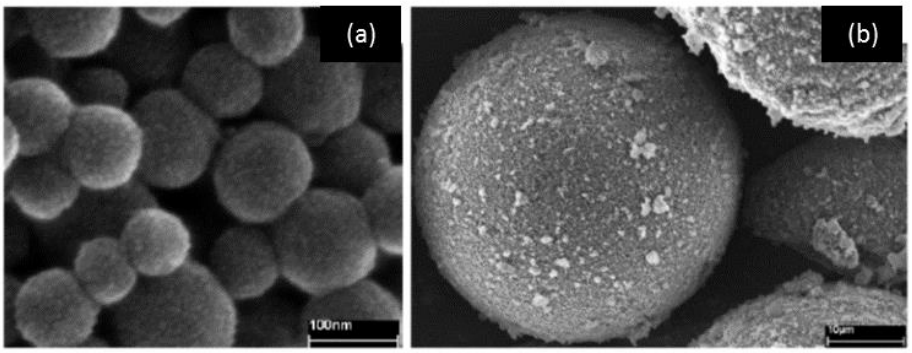


Figure 1.8. SEM images of (a) Laponite-clay-stabilized and (b) TiO2-stabilized polystyrene hybrid materials prepared using Pickering emulsion polymerization[38].

The assembly of colloidal particles at liquid-liquid interface is directly related to the interfacial free energy γ of the particle and the two liquid phases, which are shown in the Young's Equation (1.1). $\gamma_{PO}$,$\gamma_{PW}$, $\gamma_{OW}$ are the interfacial tension of the particle/oil, particle/water and oil/water interface, respectively.

$$\cos\theta = \frac{\gamma_{PO} - \gamma_{PW}}{\gamma_{OW}} \qquad (1.1)$$

Experimental studies displayed that an intermediate θ values ($60^o < \theta < 120^o$) produce the most stable Pickering emulsions. Furthermore, θ is crucial to determine the type of emulsion that is favored. Hydrophilic particles ($\theta < 90^o$) tend to be found more into aqueous phase and prefer the formation of oil-in-water (o/w) emulsion. Vice versa, hydrophobic particles ($\theta > 90^o$) stabilize water-in-oil (w/o) emulsions.

$$E_B = \pi R^2 \gamma_{OW} (1 - |1 - \cos\theta|)^2 \qquad (1.2)$$

Emulsion stabilization is strongly size dependent and radius of particle is proportional to strength of binding energies of the particle with the interface which is shown by Equation 1.2 [39]. $E_B$ is the energy of particle detachment from the interface. Hence, when the colloidal particles with a radius R : (0,01 – 10 ) μm attach to the interface with $E_B$ ($10^2$-$10^6$ $k_BT$), highly stable emulsion droplets are formed and these stable Pickering emulsions can be used as scaffolds for the synthesis of advanced supracolloidal materials such as colloidosomes, colloidal nano-composites, porous solids and foams.

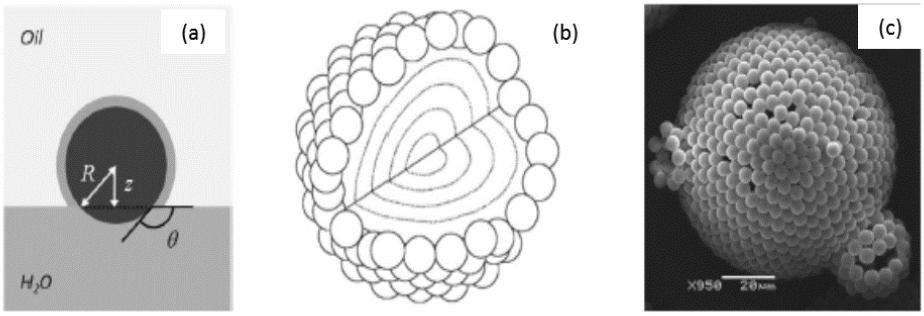


Figure 1.9. Schematic representation of Pickering stabilization and a particle that is assembled at w/o interface (a). An emulsion droplet surrounded with solid particles (b). A SEM image of a colloidal microcapsule (c)[40].

1.2.2.1. The Stability of Pickering emulsion. In principle, all emulsions are thermodynamically unstable because emulsification increases interfacial w/o area (ΔA) and that leads to increase in interfacial Gibbs free energy (ΔG) which illustrated in Equation 1.3[41]. That means all emulsions ultimately turn to two separate phases.

$$\Delta G \sim \gamma_{OW} \Delta A_{WO} \tag{1.3}$$

However, solid particles which adsorb at w/o interface decreases the w/o interfacial area; consequently, this leads to reduce ΔG and enables to obtain stable emulsions[41].

1.2.2.2. Coalescence Stability. The droplet stability of Pickering emulsion results from steric hindrance provided by the particle layer surrounding the droplet. Hence, this particle layer provides an energy barrier for coalescence which is given by Equation 1.4.

$$E_{COL} = \Delta n . E_{\boldsymbol{B}} = \Delta n . \pi R^2 \gamma_{OW} (1 - |1 - \cos\theta|)^2 \tag{1.4}$$

Equation 1.1 has already showed the calculation of $E_B$ for colloids. $E_{COL}$ becomes even larger by Δn particle, which indicates that the energetic barrier is sufficiently high to prevent coalescence[40].

### 1.2.3. Crosslinking of NPs at Liquid-Liquid Interface

Even though colloidal nanoparticles which adsorb at liquid-liquid interface stabilize emulsions, reinforcement of the particle layer surrounding the droplet is still required to obtain mechanically stable microcapsule. This can be achieved by two different ways which are via covalent interactions between NPs, and via non-covalent interactions between NPs.

1.2.3.1. Covalent Interaction between Nanoparticles. Covalent crosslinking between nanoparticles increases mechanical strength and structural stability of microcapsules. For example, stable magnetic colloidosomes were fabricated by crosslinking NPs at a water-oil interface using click chemistry [42]. In this method, alkyne- and azide-functionalized $Fe_3O_4$ NPs were assembled at the interface and Cu(I)-catalyzed Huisgen click reaction was used to link the nanoparticles between each other covalently. Hence, this method provides dense crosslinking of NPs on the colloidosome shell, which enhances the stability of colloidosomes significantly. Furthermore, alkyne and azide functional groups in click chemistry are highly selective with each other and the bond they formed is essentially inert to the many functional groups and environmental conditions such as pH and solvent.

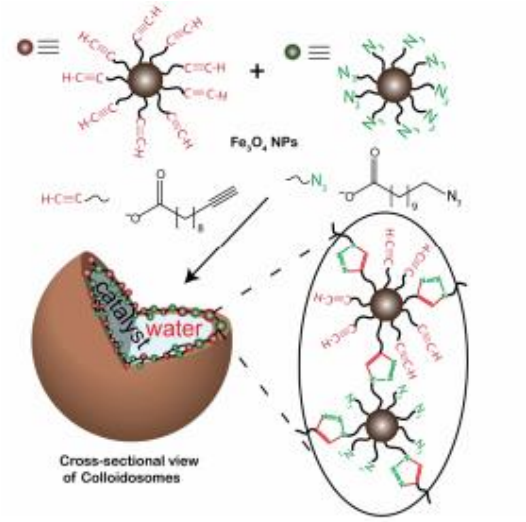


Figure 1.10. Formation of magnetic colloidosomes through self-assembly at water-in-oil interfaces followed by interfacial crosslinking of NPs via click chemistry and cross-sectional view of a colloidosome [42].

In addition to this study, stable microcapsules can be also fabricated by cross-linking between –OH group of poly(ethylene glycol) (PEG) coated onto iron oxide nanoparticle and starch modified gold nanoparticle in the presence of terephthaloyl chloride as a crosslinker(Figure 1.11). Due to the presence of both the plasmonic and magnetic nature of the constituent nanoparticles, these microcapsules could be used to explore in cancer imaging and therapy[43].

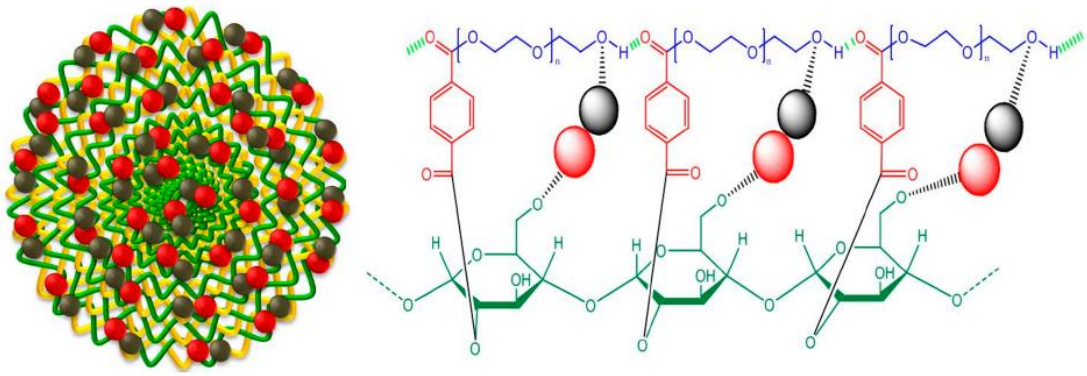

Figure 1.11 Schematic description of formation microcapsules by ligand polymerization between modified gold and iron oxide nanoparticles at the water-oil interface.

1.2.3.2. Non-Covalent Interaction between Nanoparticles. Compared to the covalent strategies, non-covalent interaction mediated self-assembly provides a unique tool for the creation of catalysts, sensors, and devices. In a recent work, Sanyal and Rotello reported that robust microcapsules were fabricated via "host-guest" type of molecular recognition at the liquid-liquid interface[15]. Water soluble β-cyclodextrin capped gold NPs was used as a guest molecule and organosoluble adamantly functionalized gold NPs were as a guest molecule, and they were crossed linked at oil-water interface to create microcapsule.

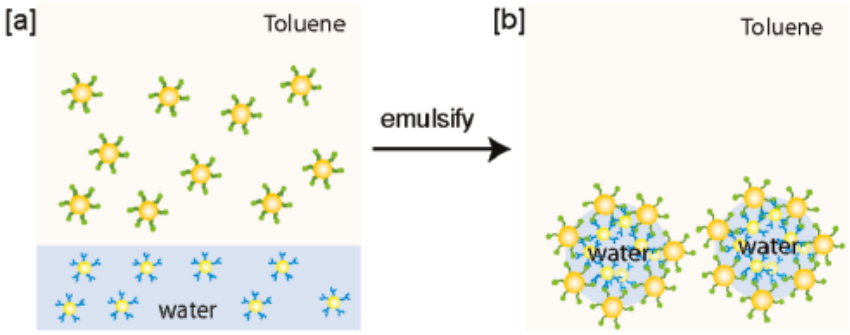


Figure 1.12. Fabrication of colloidal microcapsule via recognition mediated crosslinking.

In addition to that, divalent linker molecules can be utilized to crosslinked NPs a liquid liquid interface. Bis-adamantane containing linker molecules can be used as a guest

molecule to cross-link β-cyclodextrin capped gold NPs at oil-water interface to form stable microcapsules[44].

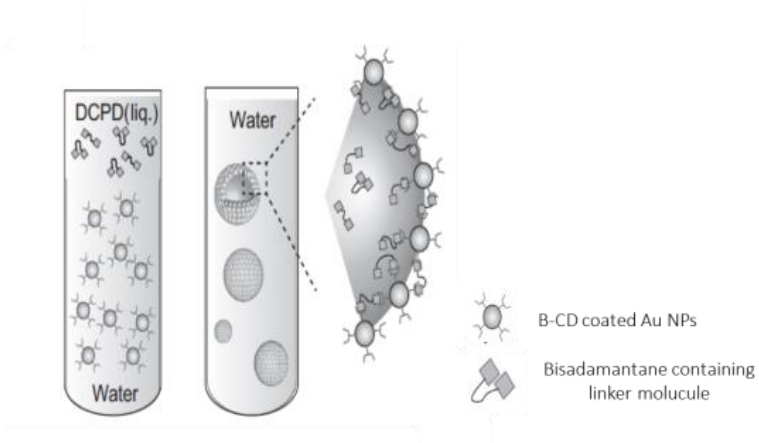


Figure 1.13. Schematic description of formation microcapsules by to crosslinking β-cyclodextrin capped gold NPs and bis-adamantane linkers at liquid-liquid interface.

### 1.2.4. Disulfide Bond-Based System

A disulfide bond is a covalent linkage which is derived from the oxidation of two thiol groups. This linkage group is also called disulfide bridge. It has two essential properties render this bond attractive in designing drug delivery systems. One of which is that it can be reversibly reduced and re-oxidized. The other is that it is relatively stable in plasma. Due to these properties of disulfide linkage, it is highly preferred to use in drug delivery system[45].

Disulfide linkages can be reduced by using different reducing agents such as dithiothreitol (DTT) and glutathione (GSH). Since glutathione is a protein naturally produced in human body and its concentration is significantly different between the extracellular and the intracellular environment. In the human body, the concentration of intracellular GSH is approximately 1−10 mM, on the other hand, it is 2−3 orders higher than that in extracellular environment (∼10 μM), such as plasma. Because of this concentration differences, a disulfide bond is stable under physiological conditions in the circulation, as well as in extracellular environment. However, it can be quickly cleaved in a highly reductive

environment within cells. Hence, this leads to achieve controlled intracellular rapid release[46]. Moreover, It is also known that the GSH concentration in tumor cells is significantly higher than that in normal cell, which made a great contribution to improve redox-responsive controlled drug delivery systems based on a disulfide cleavage trigger for cancer therapy [47].

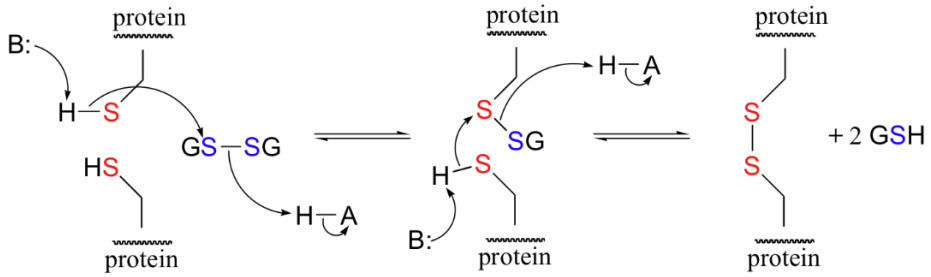


Figure 1.14. Schematic description of reduction disulfide bond by GSH.

# 2. AIM OF THE PROJECT

The main aim of the thesis is to fabricate redox-responsive colloidal microcapsule via host-guest interaction at water oil interface. The thesis divides into two parts. In the first part, bis adamantane containing linker molecules and β-cyclodextrin-coated gold nanoparticles used as guest and the host molecules, respectively in order to fabricate microcapsules. In the second part, adamantine functionalized iron oxide nanoparticles and β-cyclodextrin-coated gold nanoparticles used as the guest and the host molecules, respectively, to form microcapsules. Since the guest molecules used in the first part and second part contain redox responsive linkage, fabricated microcapsules gain the sensitivity against reducing agents.

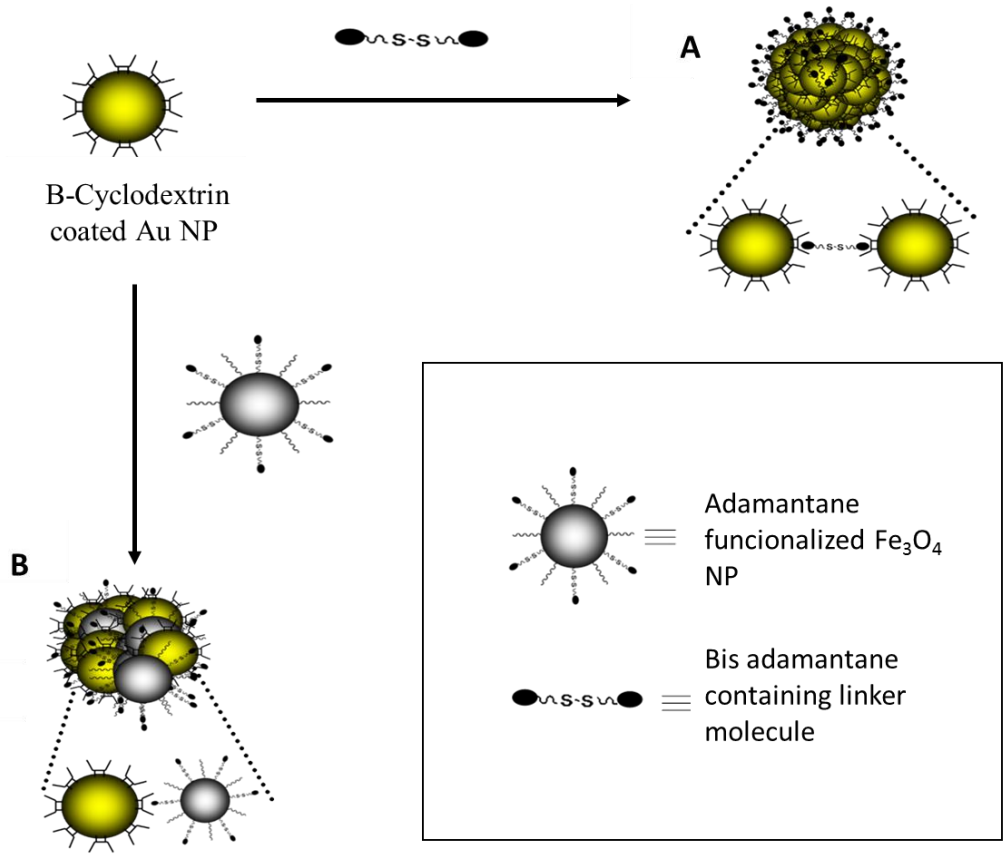


Figure 2.1. Schematic illustration of the aim of the study.

# 3. EXPERIMENTAL

## 3.1. Methods and Materials

All chemicals were reagent grade and were used as received from manufacturer (Merck, Aldrich, Alfa Aesar, and Riedel de Haen) unless otherwise noted. Dry $CH_2Cl_2$ was obtained from ScimatCo Purification System, dry DMF was dried with molecular sieves. Column Chromatography was performed using silicagel-60 (43-60 μm). Thin layer chromatography was performed using silica gel plates (Kiesel gel F254, 0.2 mm, Merck). Infrared Spectroscopy was carried out on Thermo Scientific Nicolet 380 FTIR spectrophotometer. Transmission electron microscopy (TEM), scanning electron microscopy (SEM), optical microscopy and fluorescence microscopy were used to visualize microcapsules.$^1$H NMR (operating at 400 MHz) and was recorded on Varian Mercury-MX in $CDCl_3$ as solvent at the Advanced Technologies Research and Development Center at Bogazici University.

## 3.2. Synthesis of Building Blocks

### 3.2.1. Synthesis of β Cyclodextrin Functionalized Au Nanoparticles

3.2.1.1. Synthesis of Per Iodo β-Cyclodextrin. According to a literature procedure[48], Iodine ($I_2$) (6.98 g, 27.6 mmol) was slowly added to a solution of triphenylphosphine ($Ph_3P$) (6.91 g, 26.5 mmol) in dry dimethylformamide (DMF) (30 mL). Temperature of solution was increased to 50 $^oC$. Dry β-cyclodextrin (2.00 g, 10.2 mmol) was then added to the solution. After that, temperature of the solution was increased to 70 $^oC$ and stirred for 20 h. Then, the solution was concentrated to 1/3 of its original volume. To this residue, sodium methoxide ($CH_3ONa$) in methanol (MeOH) (3.00 M, 10.3 mL) was added where the reaction was cooled in an ice/salt slurry and the mixture was stirred for 30 minuntes. After that, the reaction mixture was poured into MeOH (150 mL) to form precipitate. It was then washed

with MeOH 6-7 times by successive dispersion and centrifugations. $^1$H MNR spectrum was in agreement with the literature data.

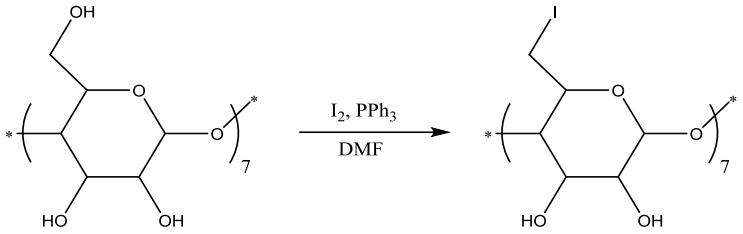


Figure 3.1. Synthesis of per iodo β-CD.

3.2.1.2. Synthesis of Per Thio β-Cyclodextrin. According to a literature procedure[49], per iodo cyclodextrin (0.500 g, 0.26 mmol ) was dissolved in DMF (6 mL). Thiourea (0,156 g, 2.05 mmol) was then added and the reaction mixture heated to 70 $^o$C under a nitrogen atmosphere. After 19 h, the DMF was removed under reduced pressure to give a yellow oil, which was dissolved in water (25 mL). Sodium hydroxide (NaOH) (0.135 g, 3.37 mmol) was added and the reaction mixture heated to a gentle reflux under a nitrogen atmosphere. After 1 h, the resulting suspension was acidified with aqueous potassium bisulfate ($KHSO_4$) and the precipitate was filtered off, washed thoroughly with distilled water, and dried. To remove the last traces of DMF, the product was suspended in water (25 mL) and the minimum amount of potassium hydroxide added to give a clear resulting fine precipitate was carefully filtered off and dried in freeze-drier. $^1$H MNR spectrum was in agreement with the literature data.

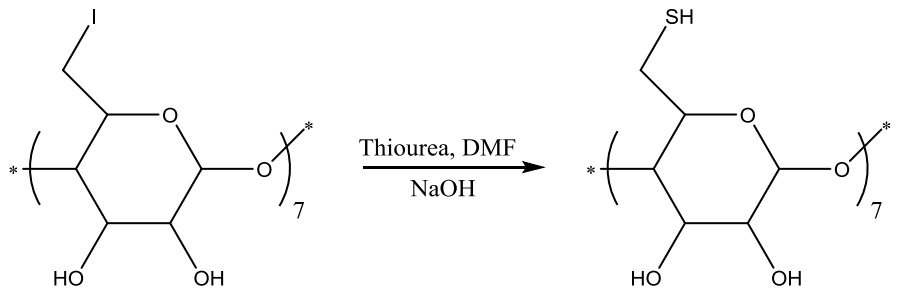


Figure 3.2. Synthesis of per thio β-CD.

3.2.1.3. Synthesis of β-Cyclodextrin Functionalized Au Nanoparticles. According to a literature procedure[50], hydrogen tetrachloroaurate (III) hydrate ($HAuCl_4$) (90 mg, 0.27 mmol) was dissolved in dimethyl sulfoxide (DMSO) (10 mL). This solution was mixed quickly with a solution of sodium borohydride ($NaBH_4$) (123 mg, 3.25 mmol) and per thio cyclodextrin (100 mg, 0.008 mmol) in DMSO (10 mL). The reaction mixture turned deep-brown immediately, and was allowed to continue for 24 h. At this point, acetonitrile ($CH_3CN$) (20 mL) was added to precipitate the nanoparticles, which were collected and purified by centrifugation, followed by washing with $CH_3CN$:DMSO (1:1 v/v, 30 mL) and ethanol (30 mL), dissolution in water, and freeze-drying. $^1H$ MNR spectrum was in agreement with the literature data.

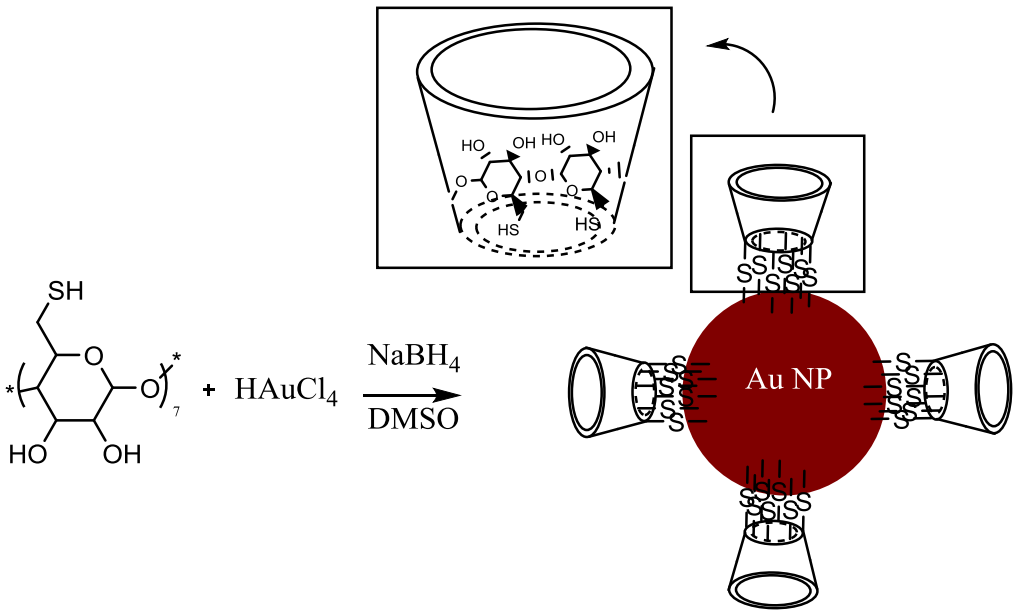


Figure 3.3. Synthesis of β-CD Functionalized Au NPs.

### 3.2.2 Synthesis of Bisadamantane Containing Linker Molecules

3.2.2.1 Synthesis of non-redox responsive bisadamantane containing linker molecule (AD-N-O-N-AD). 1-Adamantanecarbonyl chloride (500 mg, 2.25 mmol) and triethylamine (500 µL) in dry tetrahydrofuran (THF) (0.1 M) at 0 $^oC$ was added by portions the 4,7,10-trioxa-1,13-tridecanediamine (264 mg, 1.2 mmol). After stirring the mixture 1 h at same

temperature, it was warmed to RT and stirred for 17 h. THF was evaporated, then the crude was diluted with dichloromethane (DCM). The organic phase was washed with hydrochloric acid (HCl) (1 M x 4). After that it was dried over anhydrous $Na_2SO_4$ and concentrated *in vacuo*. The product was purified by column chromatography on a silica gel column. $^1$H NMR spectrum ($CDCl_3$, δ, ppm) = 6.22 (b, 1H), 3.64-3.57 (m, 4H), 3.54 (t, 2H), 2.00 (b, 3H), 1.82-1.81 (d, 6H), 1.78-1.64 (m, 8H). $^{13}$C NMR (CDCl3, δ, ppm) 177.7, 70.6, 70.5, 70.3, 40.4, 39.2, 38.0, 35.5, 29.1, 28.2. FTIR ($cm^{-1}$) 3315.7, 1626.8.

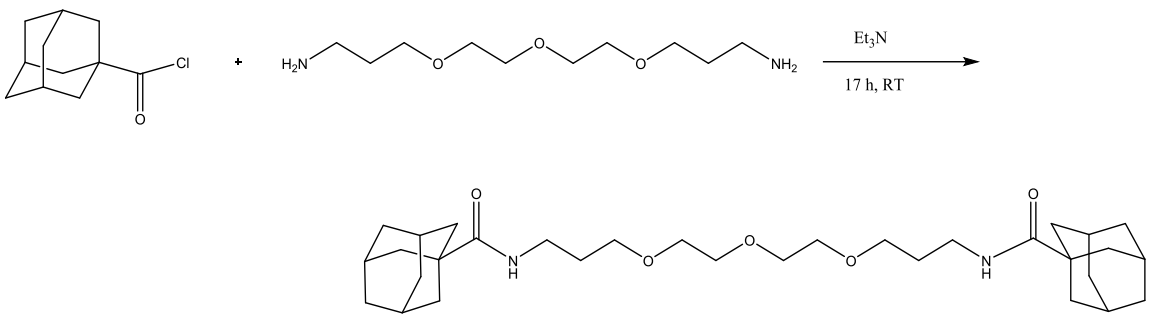


Figure 3.4. Synthesis of AD-N-O-N-AD.

3.2.2.2. Synthesis of AD-N-Boc. 1-Adamantanechloride (500 mg, 2.52 mmol) and triethylamine (416 μL) in dry THF (0.1 M) at 0 $^o$C was added by portions the N-Boc-1,6-hexanediamine (453.6 mg, 2.1 mmol). After stirring the mixture 1 h at same temperature, it was warmed to RT and stirred for 17 h. THF was evaporated, then the crude was concentrated with DCM and purified by column chromatography on a silica gel column. $^1$H NMR spectrum ($CDCl_3$, δ, ppm) = 5.62 (b, 1H), 4.53 (b, 1H), 3.23-3.18 (m, 2H), 3.11-3.06 (m, 2H), 2.02 (b, 3H), 1.83-1.82 (d, 6H), 1.74-1.65 (m, 6H), 1.48-1.42 (m, 13H), 1.32-1.28 (m, 4H).

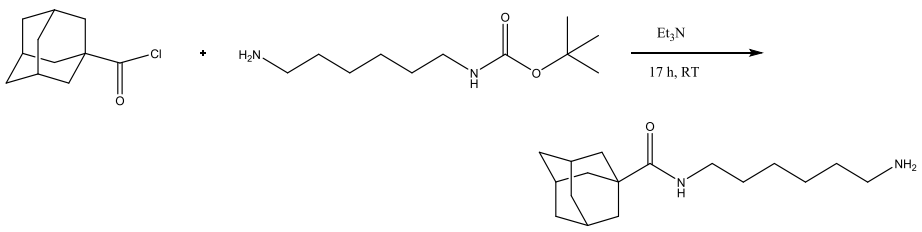


Figure 3.5. Synthesis of AD-N-Boc.

3.2.2.3. Synthesis of AD-N-$NH_2$. According to the reported article[51], (37,8 mg, 10 mmol) AD-N-Boc were dissolved in (10 mL) dry DCM and (10 mL) trifluoroacetic acid (TFA) The solution was stirred for 3 h at room temperature. Next, the solution was carefully washed five times with saturated sodium carbonate solution and then with water. The organic layer was separated and dried with anhydrous $Na_2SO_4$. After evaporation of the solvent, the final product was obtained. $^1$H NMR spectrum ($CDCl_3$, δ, ppm) = 5.54 (b, 1H), 3.24-3.20 (m, 2H), 2.67-2.64 (m, 2H), 2.01 (b, 3H), 1.83-1.82 (d, 6H), 1.70-1.68 (m, 6H), 1.48-1.43 (m, 4H), 1.30-1.23 (m, 4H).

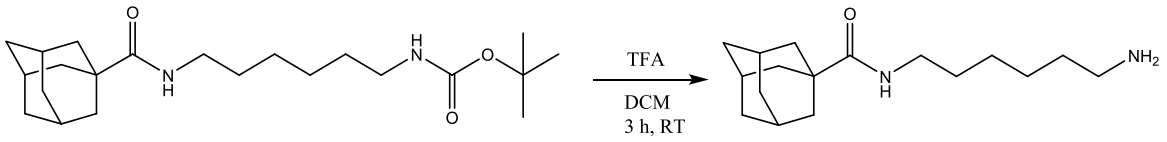


Figure 3.6. Synthesis of AD-N-$NH_2$.

3.2.2.4. Synthesis of redox responsive bisadamantane containing linker molecule (AD-N-SS-N-AD). (140 mg, 0.5 mmol) AD-N-$NH_2$, (40 mg, 0.168 mmol) 4,4'-dithiodibutyric acid, (70.7 mg, 0.369 mmol) 1-ethyl-3-(3-dimethylaminopropyl) carbodiimide (EDCI) and (4.1 mg, 0.033 mmol) 4-dimethylaminopyridine (DMAP) were dissolved in (7mL) dry DCM under nitrogen atmosphere. After that, the reaction was stirred for 20 h at RT. To purify, or with was done saturated $NaHCO_3$. Then, column chromatography was followed with 100% hexane. $^1$H NMR spectrum ($CDCl_3$, δ, ppm) = 6.26 (b, 1H), 5.69 (b, 1H), 3.23-3.17 (m, 4H), 2.72-2.63 (t, 2H), 2.32-2.28 (t, 2H), 2.02 (b, 3H), 1.83-1.82 (d, 6H), 1.74-1.65 (m, 8H), 1.49-1.44 (m, 4H), 1.35-1.23 (m, 4H). $^{13}$C NMR

178.1, 172.3, 40.5, 39.2, 39.0, 38.8, 38.3, 36.5, 34.7, 29.59, 28.1, 26.1, 26.0, 25.1. FTIR ($cm^{-1}$) 3305.3, 1631.6.

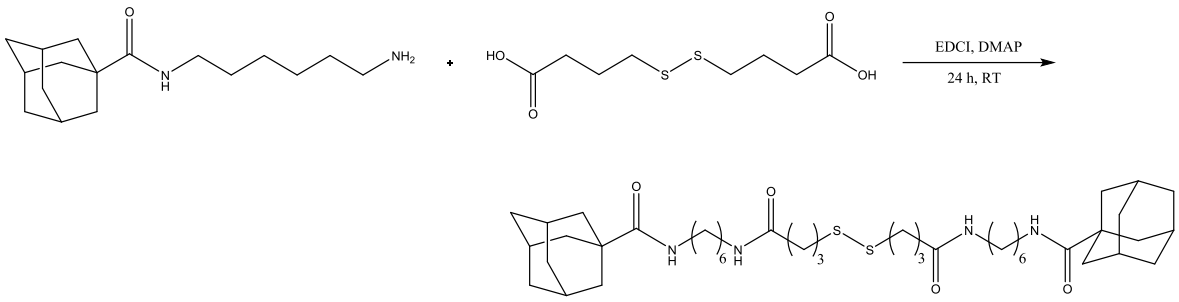


Figure 3.6. Synthesis of AD-N-SS-N-AD.

### 3.2.3. Synthesis of Adamantane Functionalized $Fe_3O_4$ Nanoparticles

3.2.3.1. Synthesis of Iron Oleate Complex. Iron oleate complex was synthesized according to the procedure reported in literature [52].

3.2.3.2. Iron Oxide Nanoparticles by Thermal Decomposition Method. Monodisperse iron oxide nanoparticles were synthesized according to reported articles[52].

3.2.3.3. Synthesis of AD-SS-$CO_2H$. (250 mg, 1.5 mmol) 1-Adamantane methanol, (1074 mg, 4.5 mmol) 4,4'-dithiodibutyric acid, (632 mg, 3.3 mmol), EDCI and (36.6 mg, 0.3 mmol) DMAP were mixed under nitrogen atmosphere. Then the mixture was dissolved in dry DCM. After that, the reaction was stirred for 24 h at RT. To purify, organic phase was washed with saturated $NaHCO_3$. Then, column chromatography was followed with 100% hexane. $^1H$ NMR spectrum ($CDCl_3$, δ, ppm) = 3.67 (s, 2H), 2.72 (t, 4H), 2.45 (t, 4H), 2.06-2.00 (m, 7H), 1.74-1.62 (dd, 6H), 1.55 (d, 6H). $^{13}C$ NMR 178.0, 173.2, 73.7, 39.3, 37.9, 37.6, 36.9, 33.1, 32.7, 32.2, 28.0, 24.3, 23.8. FTIR ($cm^{-1}$) 1731.1, 1704.9.

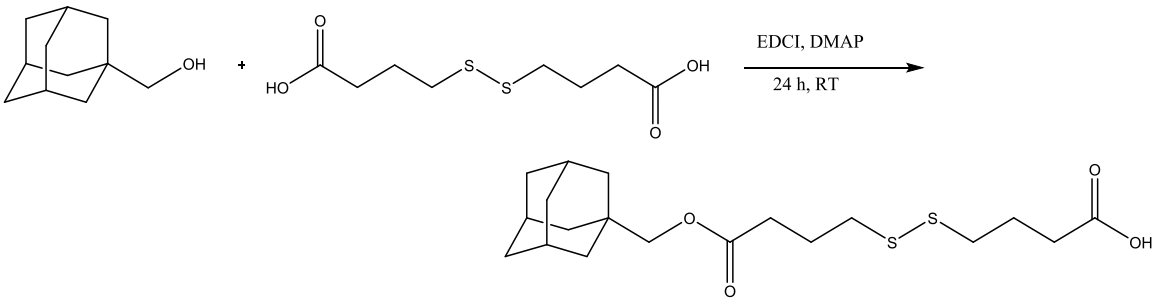


Figure 3.7. Synthesis of AD-SS-$CO_2H$.

3.2.3.4. Place Exchange Reaction to Get Redox Responsive Adamantane Functionalized Iron Nanoparticles (AD-SS-$Fe_3O_4$). Oleic acid coated iron oxide nanoparticles (50 mg) are dissolved in 1 mL DCM. 150 mg AD-SS-$CO_2$ is dissolved in 1.5 mL DCM. Two solutions are mixed and nitrogen is purged. To purify, nanoparticles are precipitated twice in ethanol and collected with the aid of a magnet. Purified ADA coated iron nanoparticles are kept in DCM.

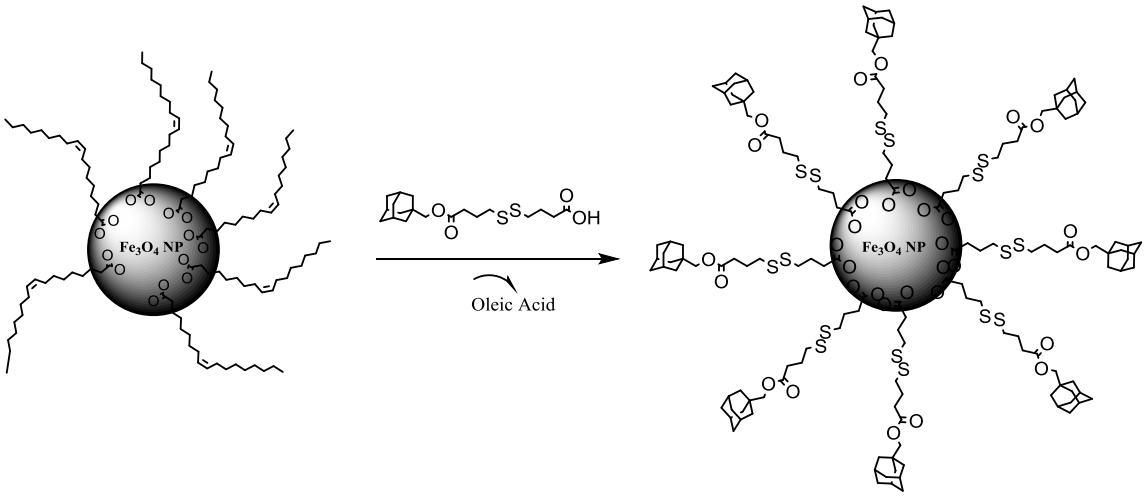


Figure 3.8. Synthesis of redox responsive adamantine functionalized iron oxide nanoparticles (AD-SS-$Fe_3O_4$).

3.2.3.5. Place Exchange Reaction to Get Non-Redox Responsive Adamantane Functionalized Iron Nanoparticles (AD-$Fe_3O_4$). Oleic acid coated iron oxide nanoparticles (50 mg) are dissolved in 1 mL DCM. 150 mg adamantine 1-carboxylic acid is dissolved in 1.5 mL DCM. Two solutions are mixed and nitrogen is purged. To purify, nanoparticles are

precipitated twice in ethanol and collected with the aid of a magnet. Purified ADA coated iron nanoparticles are kept in DCM.

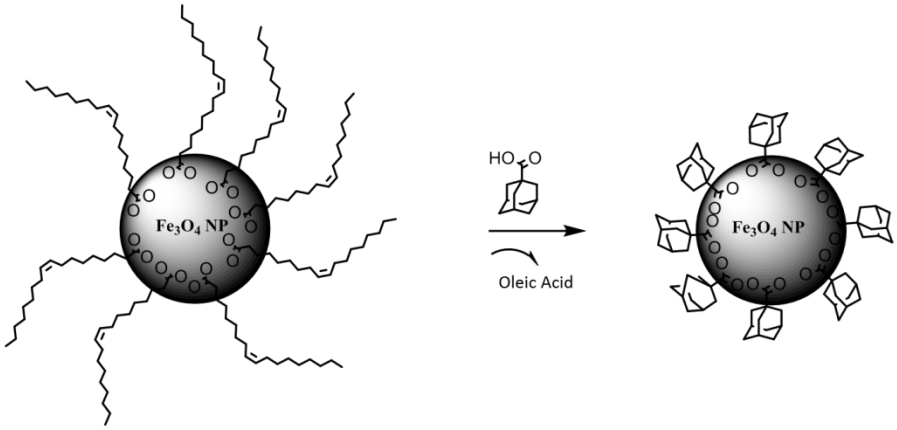


Figure 3.9. Synthesis of non-redox responsive adamantine functionalized iron oxide nanoparticles (AD-$Fe_3O_4$).

# 4. RESULTS AND DISCUSSIONS

Stable microcapsules were fabricated by using non-covalent crosslinking host and guest molecules at interface between water-organic solvent. As a host molecule, β-cyclodextrin coated gold nanoparticles and as a guest molecule, bis-adamantane containing linker molecules (AD-N-O-N-AD and AD-N-SS-N-AD) and adamantane functionalized iron oxide nanoparticles (AD-SS-$Fe_3O_4$ and AD- $Fe_3O_4$) were synthesized. Some of our guest molecules contain disulfide linkage (AD-N-SS-N-AD and AD-SS-$Fe_3O_4$), microcapsules that contain those guest groups have a sensitivity towards reducing agent such as DTT. Fabricated microcapsules were visualized under optical microscope. Then fluorescence dye were encapsulated into them. Their stability towards DTT were analyzed by using fluorescence microscope.

## 4.1. Fabrication of Microcapsules by Using β-Cyclodextrin Coated Au NPs and Bisadamantane Containing Linker Molecules

### 4.1.1. Functionalization of Au Nanoparticles

Water soluble β-cyclodextrin coated Au NPs were synthesized according to procedure described before. They were visualized under TEM (Figure 4.1a). Furthermore, size of NPs were measeure by dynamic light scattering (DLS), and average particle size was found to be about 6 nm (Figure 4.1b). In addition to that, their UV-Vis spectum was taken and maximum absorption peak was observed around 545 nm (Figure 4.2.).

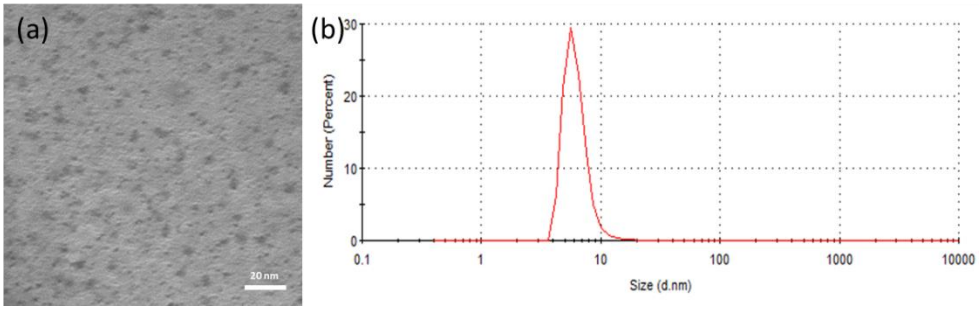


Figure 4.1. TEM image and Dynamic light scattering of β-cyclodextrin coated Au NPs, (a,b) respectively.

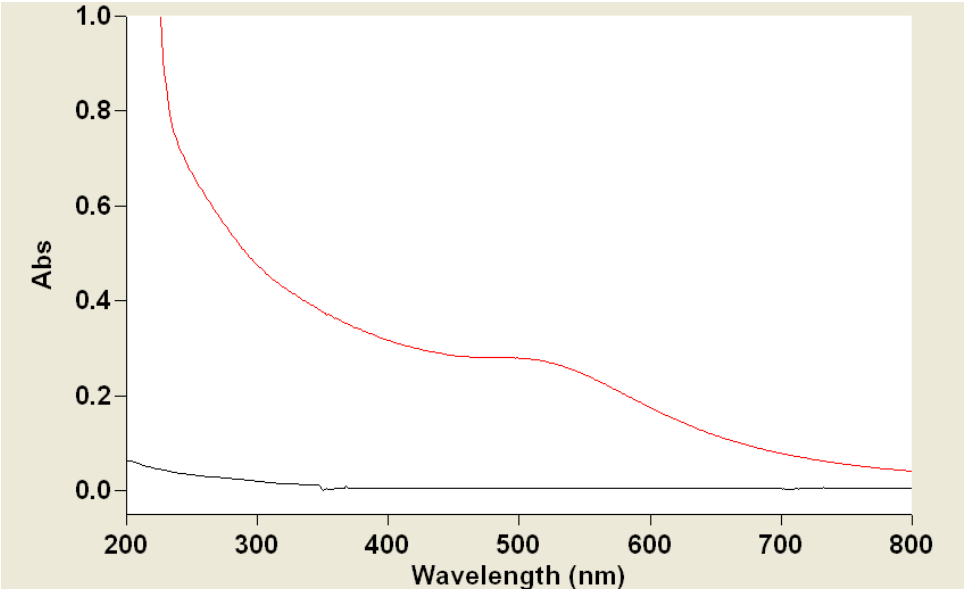


Figure 4.2. UV-Vis spectrum of β-cyclodextrin coated Au NPs

### 4.1.2. Bisadamantane Containing Linker Molecules

In this study, two different bis-adamantane containing molecules were synthesized. One is redox responsive bis-adamantane containing linker molecule since it has a disulfide bond (Figure 4.3a). The other were synthesize as a control group which is non-redox responsive bis-adamantane containing linker molecule. It does not contain any redox responsive linkage (Figure 4.3b).

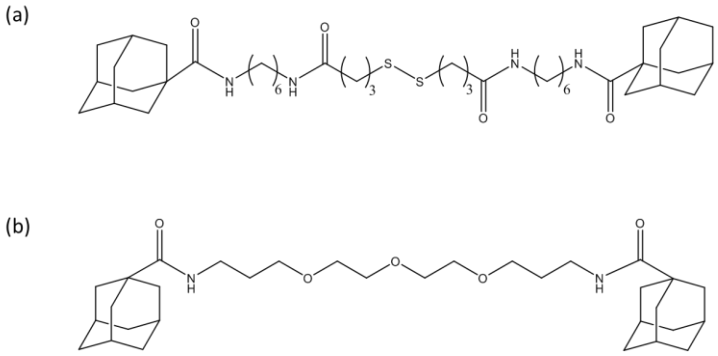


Figure 4.3. Structure of redox responsive bis-adamantane containing linker molecule (a) and non-redox responsive bis-adamantane containing linker molecule (b).

### 4.1.3. Synthesis of Microcapsules

β-cyclodextrin coated Au NPs dissolved in water (4 mg/2 mL) and 30 mM bis-adamantane containing solution in α,α,α-trifluorotoluene was prepared. Then, 100 μL of α,α,α-trifluorotoluene solution was added into the 2 mL water solution in a vial. This mixture was mixed vigorously for 30 seconds. After waiting for a few minutes, the water phase was cleaned with fresh water carefully with the help of a pipette. As a result, stable microcapsules were obtained at the bottom of the vial, and hereafter this microcapsule system is referred as α,α,α-trifluorotoluene-in-water system.

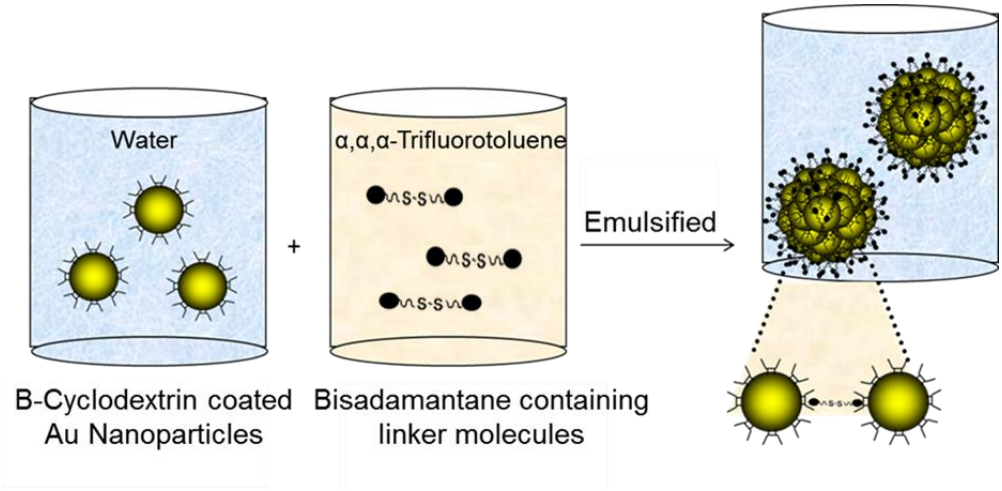


Figure 4.4. Schematic illustration of formation microcapsules in α,α,α-trifluorotoluen-in-water system.

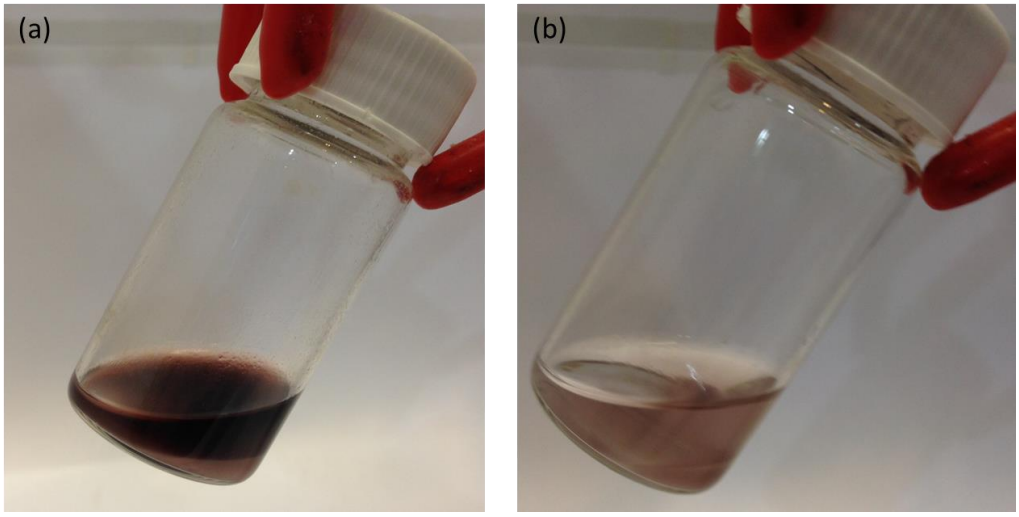


Figure 4.5. Microcapsules before (a) and after (b) cleaning of the media.

Stable microcapsules were fabricated by using AD-N-SS-N-AD and β-cyclodextrin coated Au NPs and by using AD-N-O-N-AD and β-cyclodextrin coated Au NPs. These microcapsules stayed stable in water solution at least two weeks and they were visualized under optical microscope (Figure 4.6.). They have spherical shape and their sizes are around between 20-50 μm.

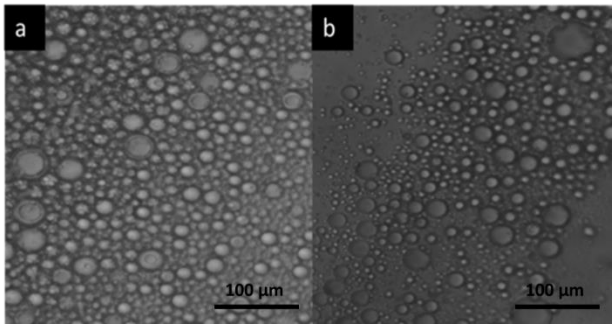


Figure 4.6. Optical image of microcapsules were formed by using AD-N-SS-N-AD and β-cyclodextrin coated Au NPs (a) and by using AD-N-O-N-AD and β-cyclodextrin coated Au NPs (b).

### 4.1.4. Encapsulation of Fluorescent Dye into the Microcapsules

Encapsulation of hydrophobic molecules into the microcapsules is possible. In order to show that, Nile red dye was encapsulated into the capsules. During the fabrication of microcapsules via α,α,α-trifluorotoluene in water system, a few drops from the Nile red

solution (2mg/mL) were added and the vial was shaken. Encapsulation of hydrophobic fluorescent dye was visualized under fluorescent microscope (Figure 4.7.).

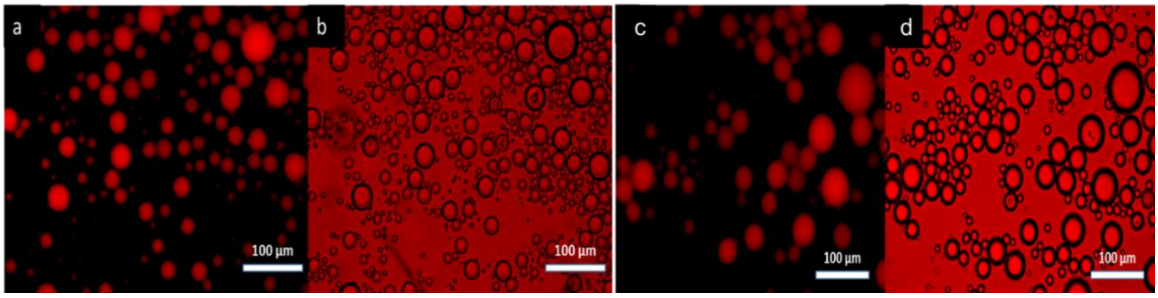


Figure 4.7. Images of Nile red dye encapsulated microcapulses which contain AD-N-SS-N-AD (a,b) and AD-N-O-N-AD (c,d) under fluorescence and optic microscopes respectively.

### 4.1.5. Controlled Dye Release from Microcapsules

Nile red dye encapsulated microcapsules which were formed by using β-cyclodextrin coated Au NPs and AD-N-SS-N-AD linker molecules were disturbed after exposing to DTT. Almost all of them were destroyed in a minute and the dye inside them were released (Figure 4.8).

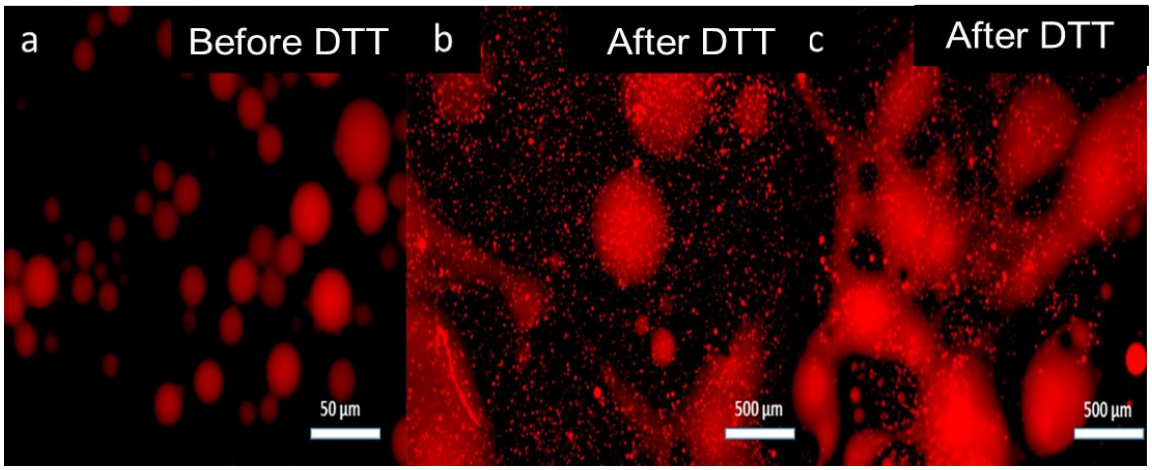


Figure 4.8. Release of red Nile dye encapsulated redox responsive microcapsules under fluorescence microscope before and after exposing to DTT.

However, microcapsules which do not contain any redox responsive linkage groups were not disturbed even after exposing to DTT. They were stable at least during 10 minutes. This process was visualized under fluoresencent microscope (Figure 4.9.).

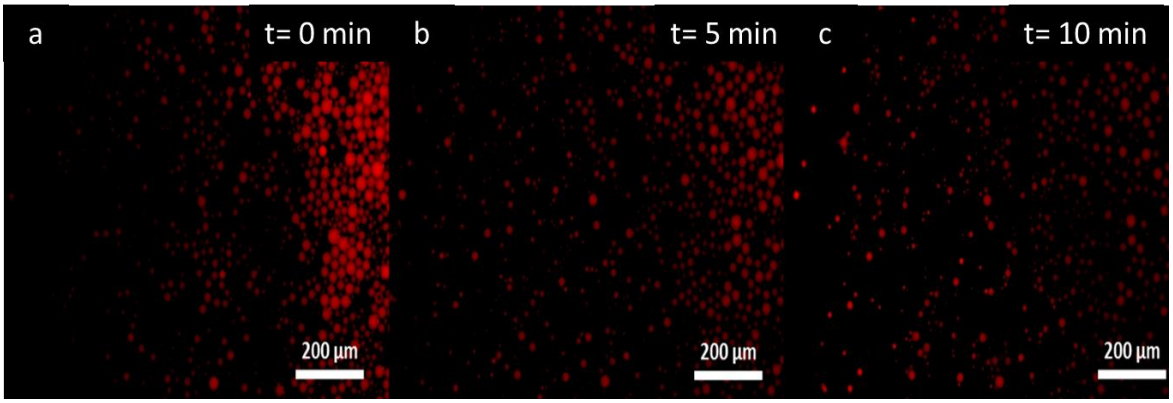


Figure 4.9. Images of red Nile dye encapsulated non- redox responsive microcapsules under fluorescence microscope after exposing to DTT.

Microcapsules were also visulaized under TEM. Their sizes were observed around 20 µm (Figure 4.10.).

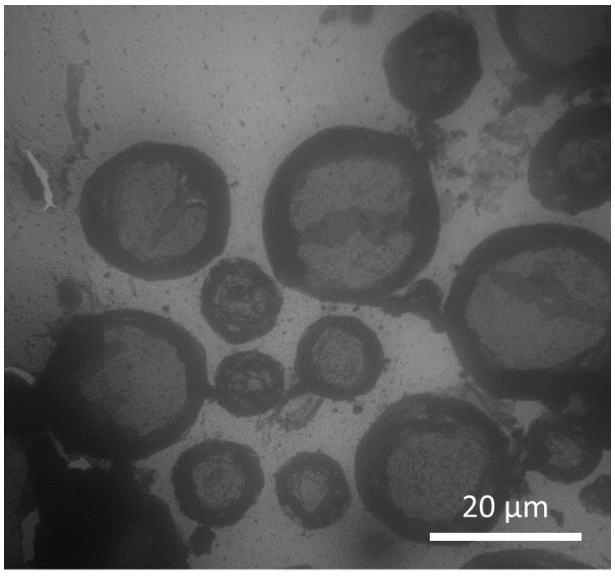


Figure 4.10. TEM images of microcapsules.

### 4.1.6. Inner Phase Polymerization of Microcapsules

Microcapsules which were fabricated by using bis-adamantane containing linker molecules and β-cyclodextrin coated Au NPs were stable in the solution. When they left outside for drying, most of the microcapsule were disturbed due to evaporation of the inner phase. However, cross-linked polymerization in the inner phase of the microcapsules provides extra stability; therefore, they are stable even though inner phase of them were evaporated. For that purpose, dicyclopentadiene were used as a monomer and by using 1st Grubbs Catalyst cross-linked polymerization was achieved.

4.1.6.1. Fabrication of the Microcapsules. According to reporting article[44], 2 mg β-cyclodextrin coated Au NPs dissolved in 0.5 mL of $H_2O$. 95 µL of the 5 µM linker in dicyclopetadiene (DCPD), 5 µL of 1.5 % (w/w) first-generation Grubbs catalyst in chloroform, and water solution were mixed by sonicator for 2 minutes. Then, the water phase was washed with fresh water. After 4 h, the inner phase was completely polymerized (Figure 4.11.). The solutions were drop-cast onto an aluminium surface and dried for 24 h under ambient conditions for SEM.

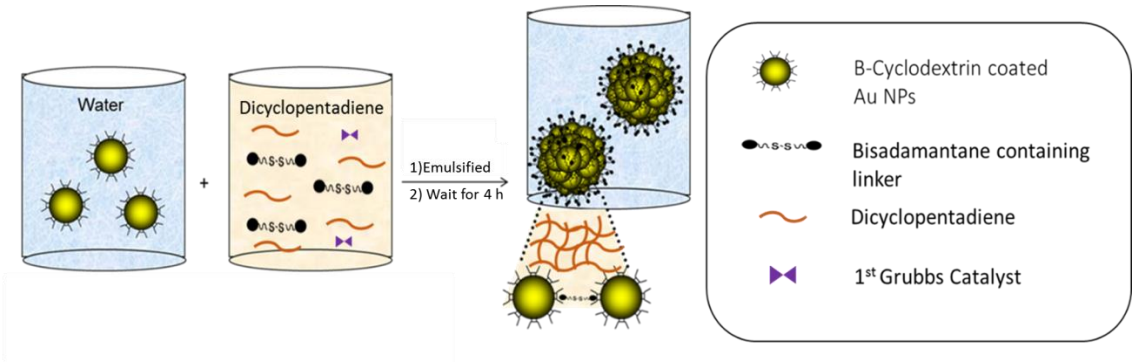


Figure 4.11. Schematic illustration of formation of inner phase polymerization of microcapsules.

After polymerization of inner phase of microcapsules were completed, they were visualized under optical microscope. Their size were observed around 20 μm (Figure 4.12a). After those microcapsules left outside for drying during 24 h, they were visualized under SEM (Figure 4.12b). It was observed that most of the microcapsules kept their spherical shape as an intact.

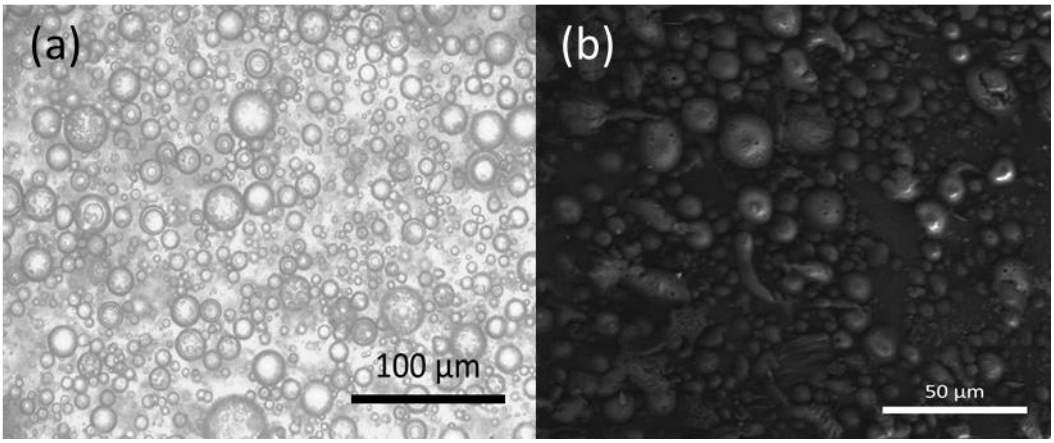


Figure 4.12. Images of the microcapusles after completing polymerization of their inner phase under optical microscope (a) and SEM (b).

## 4.2. Fabrication of Microcapsules by Using β-Cyclodextrin Coated Au NPs and Adamantine Functionalized Iron Oxide Nanoparticles

### 4.2.1. Adamantane Functionalized Iron Oxide Nanoparticles

In this study, two different adamantine functionalized iron oxide nanoparticles were synthesized. The first one contains disulfide bonds (AD-SS-$Fe_3O_4$); therefore it is redox responsive (Figure 4.13a) and the second one was synthesized as a control group (AD-$Fe_3O_4$); therefore, it does not contain any redox responsive group (Figure 4.13b). Then, it is aimed to use those adamantane functionalized iron oxide nanoparticles as a guest molecules in order to enable the fabricated microcapsules to have magnetic properties.

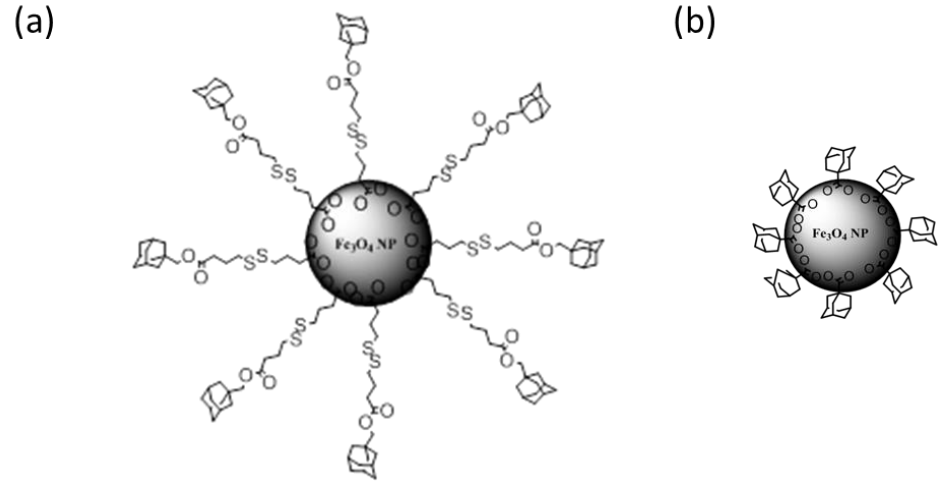


Figure 4.13. (a) Structure of redox responsive adamantane functionalized iron oxide nanoparticles, and (b) non-redox responsive adamantane functionalized nanoparticles.

Synthesis of adamantane functionalized iron oxide nanoparticles was achieved by place exchange reaction of oleic acid coated iron oxide nanoparticles with adamantane containing linker molecules. FTIR analysis of oleic acid coated iron oxide nanoparticles (Oleic Acid-$Fe_3O_4$) was completed (Figure 4.14). After place exchange reaction, non-redox responsive adamantane functionalized nanoparticles (AD-$Fe_3O_4$ NPs) were also analyzed with FTIR and they did not show any carbonyl peak in the FTIR spectrum since the linker molecule attached to the surface of the nanoparticles from its carboxyl group (Figure 4.13b). However, redox responsive adamantane functionalized iron oxide nanoparticles (AD-SS-$Fe_3O_4$ NPs) displays a carbonyl peak around 1700 $cm^{-1}$ which belongs to the carbonyl group close to the adamantyl group of the linker molecule (Figure 4.13a). Consequently, FTIR results indicated that oleic acid molecules which attached to the surface of the iron oxide nanoparticles were successfully place exchanged with redox responsive adamantane containing linker molecules or non-redox responsive adamantane containing linker molecules.

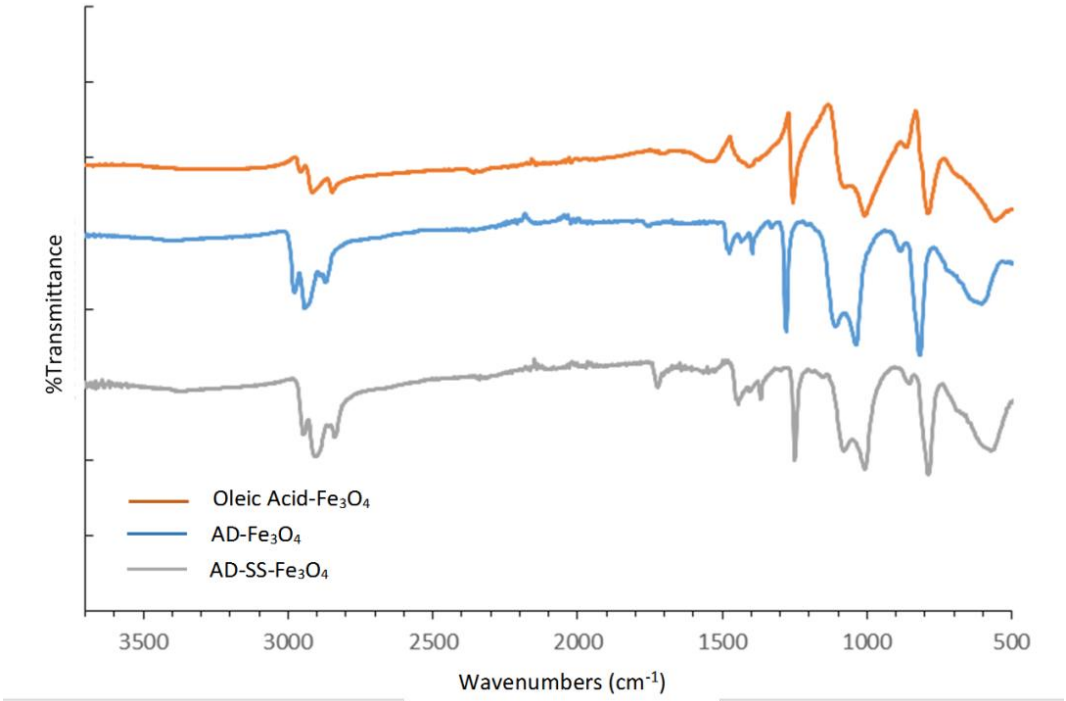


Figure 4.14. FTIR spectra of Oleic Acid-$Fe_3O_4$, AD-$Fe_3O_4$, and AD-SS-$Fe_3O_4$.

Average size of the parent oleic acid coated iron oxide nanoparticles was measured as around 10 nm by dynamic light scattering (Figure 4.15a). After place exchange reactions, average size of redox responsive adamantane coated iron oxide nanoparticles were also around 10 nm (Figure 4.15b). Also, the average size of non-redox responsive adamantane coated iron oxide nanoparticles were around 10 nm (Figure 4.15c). In addition, before and after place exchange reaction, nanoparticles were visualized under TEM. Size of the parent oleic acid coated iron oxide nanoparticles, redox responsive adamantane coated iron oxide nanoparticles and non-redox responsive adamantane coated iron oxide nanoparticles were around 10 nm (Figure 4.16.). Their shapes were similar, which demonstrated also that place exchange reactions did not lead to any unwanted agglomerations.

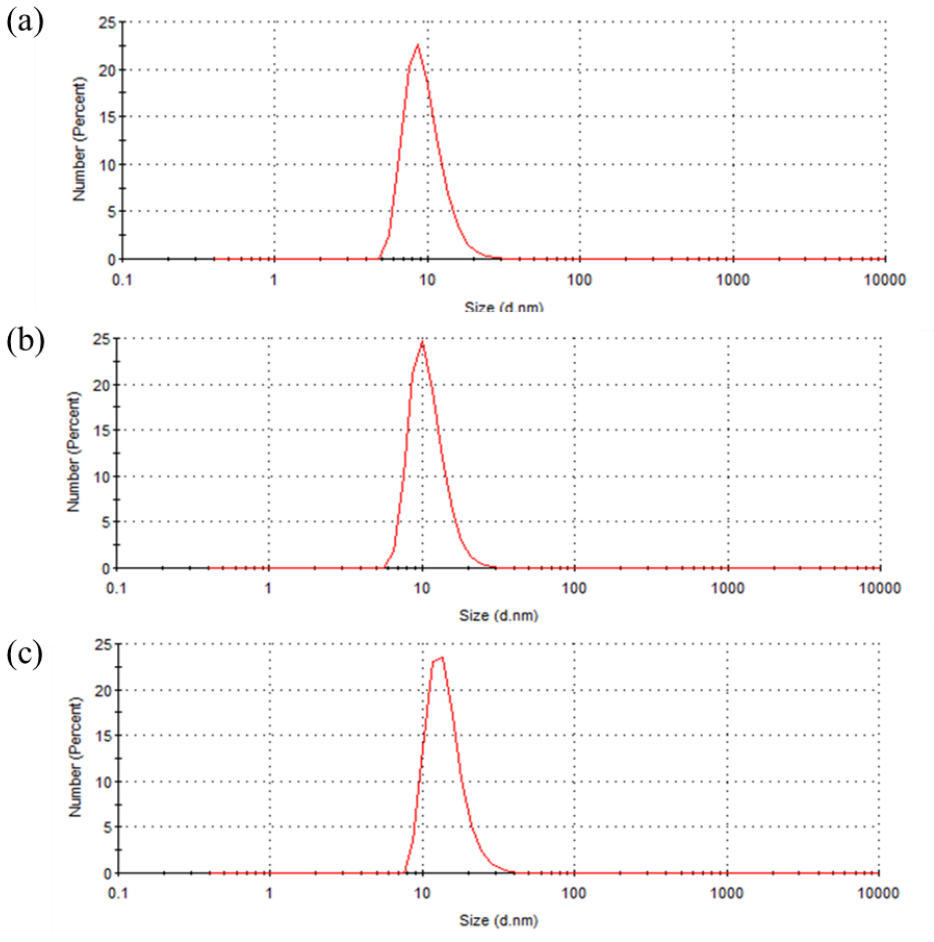


Figure 4.15. Dynamic light scatterings of Oleic Acid-$Fe_3O_4$ (a), AD-$Fe_3O_4$ (b), and AD-SS-$Fe_3O_4$ (c).

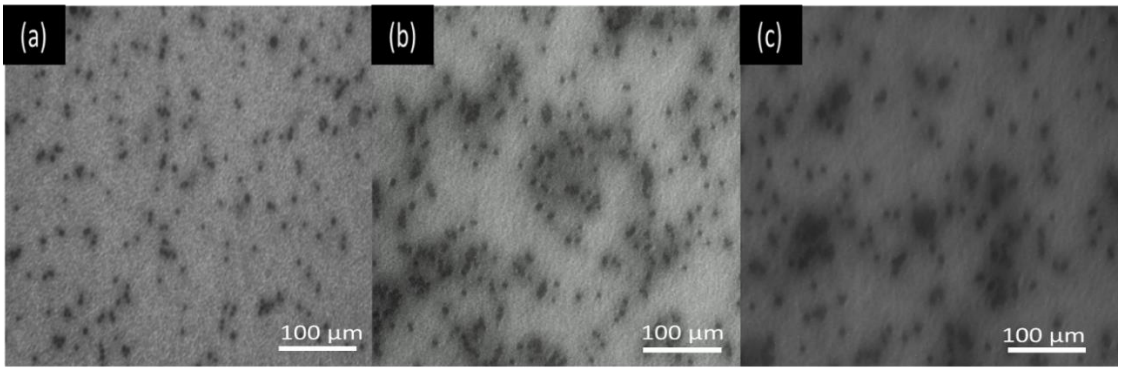


Figure 4.16. TEM images of Oleic Acid-$Fe_3O_4$ (a), AD-$Fe_3O_4$ (b), and AD-SS-$Fe_3O_4$ (c).

### 4.2.2. Phase Transfer Experiment

Adamantane functionalized iron oxide nanoparticles were soluble in organic phase. After they are exposed to reducing agent such as DTT, disulfide bonds of redox responsive iron oxide nanoparticles would cleave and the nanoparticles should become water soluble. Furthermore, DTT should not have any effect on non-redox responsive iron oxide nanoparticles; therefore, they kept on staying in organic phase. To demonstrate that this was indeed the case, phase transfer experiments were undertaken. In vial 1, non-redox responsive adamantane functionalized iron oxide nanoparticles (AD-$Fe_3O_4$) were dissolved in DCM and water was added onto this phase. In vial 2, redox-responsive adamantane functionalized iron oxide nanoparticles (AD-SS-$Fe_3O_4$) were dissolved in DCM and water was added onto this phase. After addition DTT to each of these mixtures, it was observed that while iron oxide nanoparticles in vial 1 stayed in the DCM phase, iron oxide nanoparticles were transferred to the water phase in vial 2. This indicates that a thiol-based reducing agent like DTT successfully cleaves the disulfide bond of redox responsive adamantane functionalized iron oxide nanoparticles (Figure 4.17.).

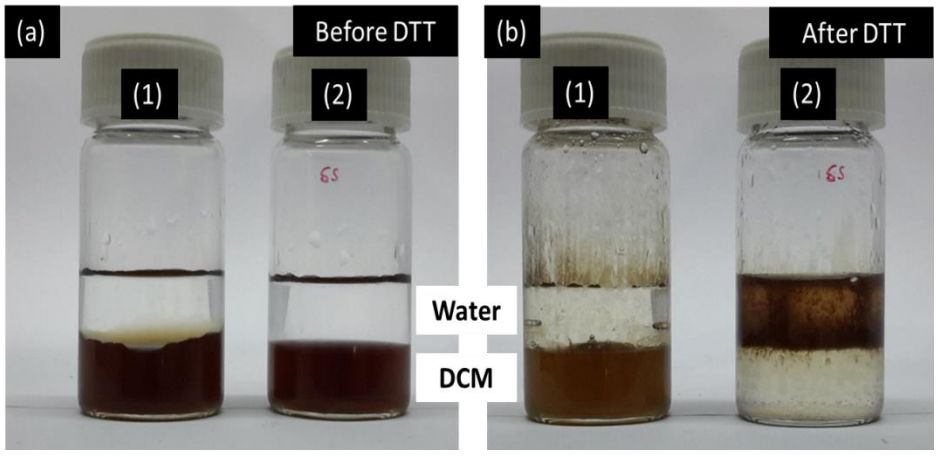


Figure 4.17. Photograph of AD-SS-$Fe_3O_4$ NPs in DCM-water mixture in vial 1 and AD $Fe_3O_4$ NPs in DCM-water mixture in vial 2 before (a) and after DTT addition (b).

### 4.2.3. Synthesis of Microcapsules

β-cyclodextrin coated Au NPs were dissolved in water (10 mg / 2 mL). Separately adamantane functionalized iron oxide nanoparticles were dissolved in DCM (6 mg /1 mL). Then, 200 µL of the DCM solution was added into 2 mL aqueous solution. This mixture was mixed vigorously for 30 seconds. After waiting for few minutes, aqueous phase was cleaned with fresh water carefully with the help of a pipette. As a result, stable microcapsules were obtained at the bottom of the vial and hereafter these microcapsule systems are referred as dichloromethane-in-water system (Figure 4.18.).

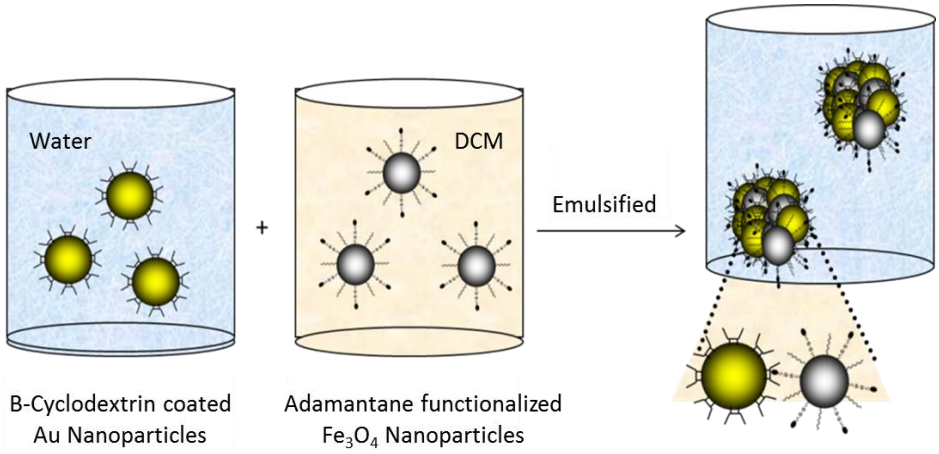


Figure 4.18. Schematic illustration of formation microcapsules in DCM-in-water system.

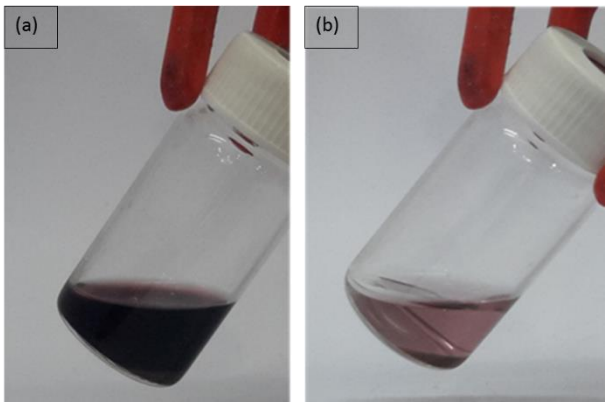


Figure 4.19. Microcapsules (a) before, and (b) after cleaning of aqueous media.

Stable microcapsules were fabricated by using redox responsive iron oxide nanoparticles and β-cyclodextrin coated Au NPs and by using non-redox responsive iron oxide nanoparticles and β-cyclodextrin coated Au NPs. These microcapsules stayed stable in water solution at least two weeks and they were visualized under optical microscope (Figure 4.20.). They were spherical in shape and their sizes are between 20-50 μm.

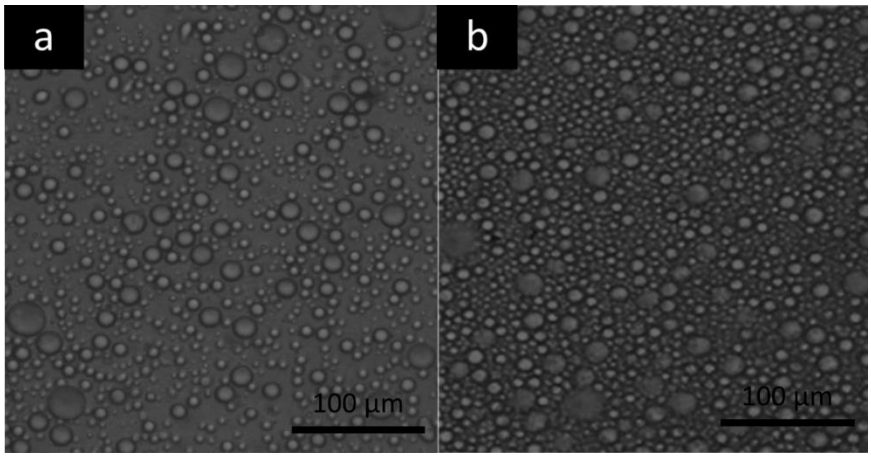


Figure 4.20. Optical image of microcapsules were formed by using redox responsive iron oxide nanoparticles and β-cyclodextrin coated Au NPs (a) and by using non-redox responsive iron oxide nanoparticles and β-cyclodextrin coated Au NPs (b).

### 4.2.4. Destruction of Redox Responsive Microcapsules with DTT

Microcapsules which were formed by using β-cyclodextrin coated Au NPs and redox responsive adamantane functionalized iron oxide nanoparticles were visualize under optical microscope at 0, 5 and 10 minutes. It is clearly seen that most of the microcapsules were stable under the microscope. However, some microcapsules broke over time due to evaporation DCM inside the microcapsules. Moreover, light of the microscope also increases the temperature, which decreases the stability of microcapsules in the solvent. Nevertheless, most of the microcapsules were stable during the duration of experiments (10 mins) (Figure 4.21.).

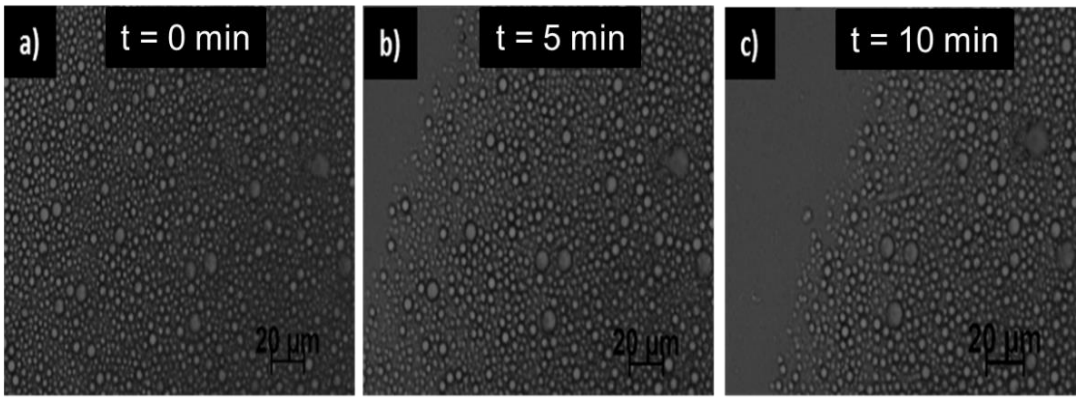


Figure 4.21. Images of microcapsules under optical microscopes at t = 0, 5, 10 minutes (a, b, c respectively).

However, microcapsules which were formed by using β-cyclodextrin coated Au NPs and redox responsive adamantane functionalized iron oxide nanoparticles were destroyed after they were exposed to DTT. As observed under optical microscope, all microcapsules were disrupted within 3 minutes (Figure 4.22.).

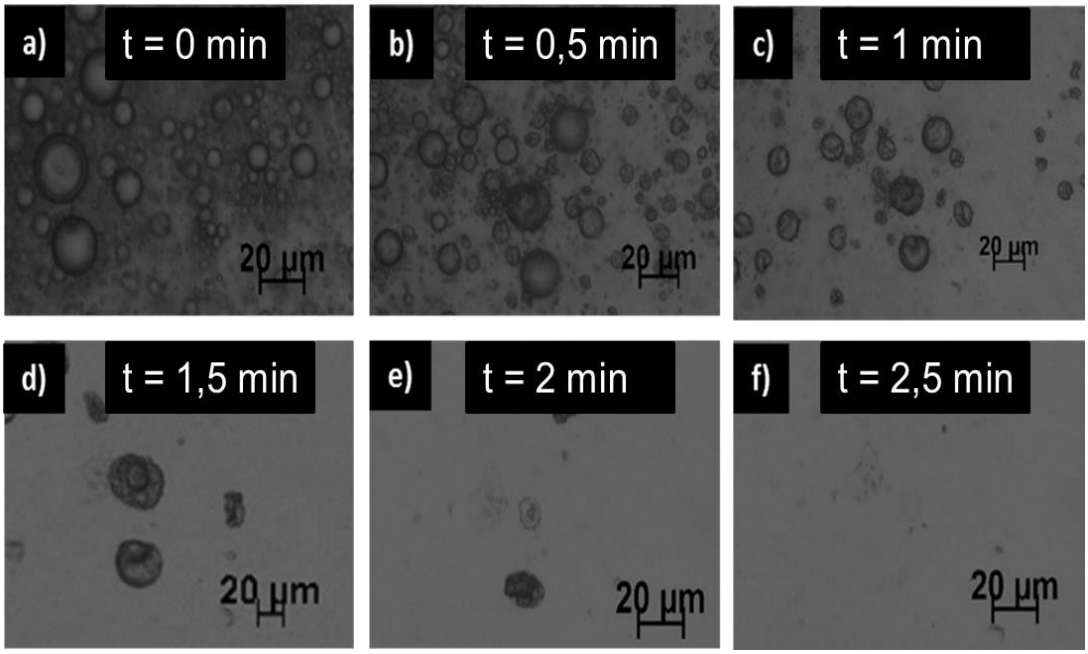


Figure 4.22. Images of microcapsules after exposing DTT under optical microscopes at t=0, 0.5, 1, 1.5,2 and 2.5 minutes (a, b, c, d, e, f respectively).

### 4.2.5. Controlled Dye Release from Microcapsules

Nile-red dye encapsulated microcapsules which were formed by using β-cyclodextrin coated Au NPs and redox responsive iron oxide nanoparticles were also disrupted after exposing to DTT. Almost all of them were destroyed in a minute and the dye inside them were released (Figure 4.23.).

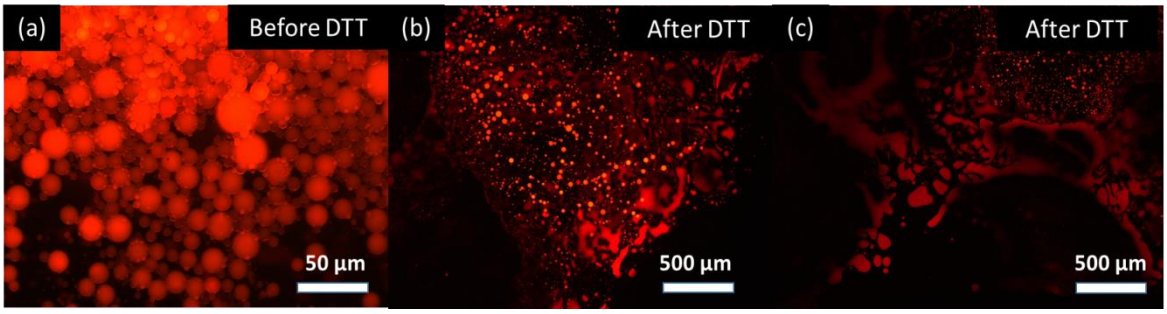


Figure 4.23. Release of red Nile dye encapsulated redox responsive microcapsules under fluorescence microscope after exposing to DTT.

However, microcapsules which did not contain the redox responsive linkage groups were not disturbed even after exposing to DTT. They were stable at leeast during 10 minutes. This process is visualized under fluoresencent microscobe (Figure 4.23.).

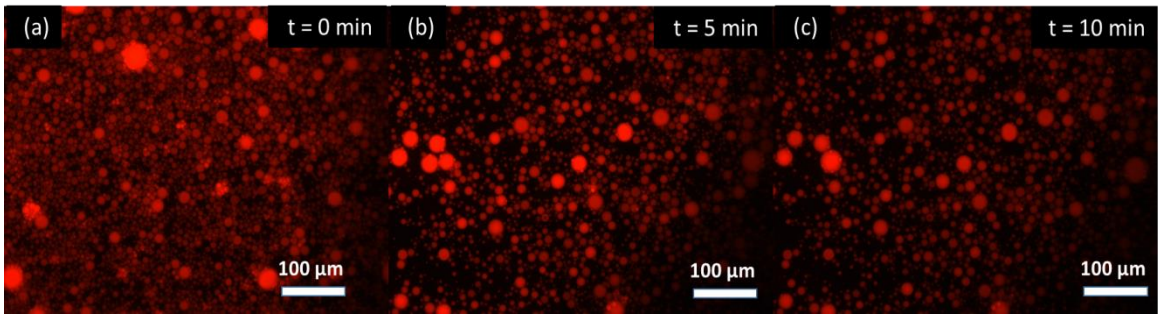


Figure 4.24. Images of red Nile dye encapsulated non- redox responsive microcapsules under fluorescence microscope after exposing to DTT.

### 4.2.6. Magnetic Properties of Microcapsules

Microcapsules which contain adamantane functionalized iron oxide nanoparticles display magnetic properties. Their position can be changed when they exposed to magnetic field. When a magnet was brought close to the microcapsule solution, the movement of the microcapsules toward the magnet was observed (Figure 4.25.)

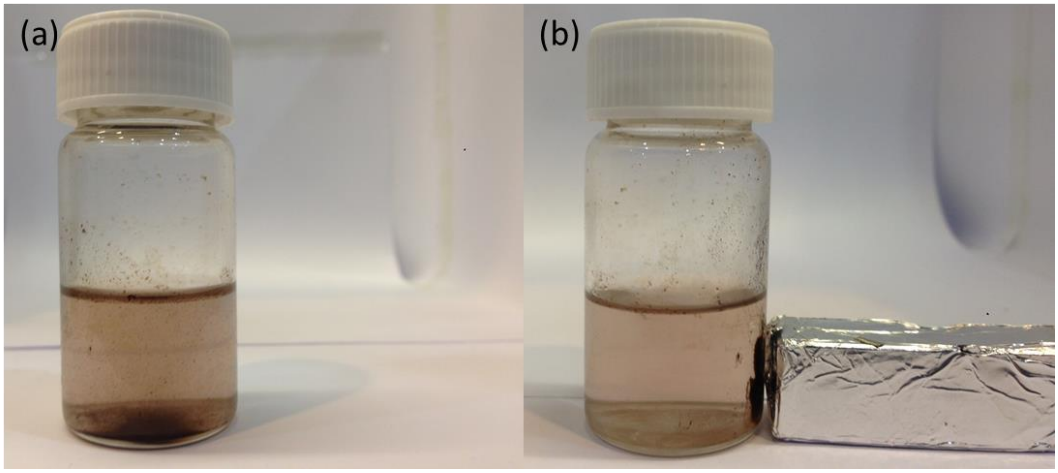


Figure 4.25. Positions of microcapsules in the solution with magnetic field.

### 4.2.7. Post-Modification of Surface of Microcapsules

After fabrication of microcapsules via DCM in water system, a drop of adamantane functionalized lissamine dye solution in water was added. Due to the presence of the adamantane functionality on the dye, host-quest interactions with cyclodextrin groups on the microcapsule surface can occur. Hence the dye gets localized on the surface of the microcapsules, which was visualized under fluorescent microscope (Figure 4.26.). This demonstrates that the surface functionality of these microcapusles can be tailored using appropriately functionalized ligands.

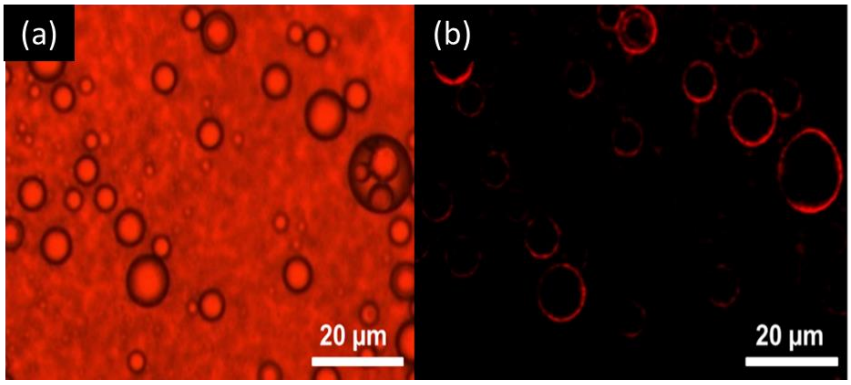


Figure 4.26. The image of microcapsules encapsulating adamantane functionalized lissamine dye at the cross section under (a) optical and (b) fluorescence microscopes.

### 4.2.8. Inner Phase Polymerization of Microcapsules

β-cyclodextrin coated Au NPs was dissolved in water (2 mg/ 1 mL). AD-SS-$Fe_3O_4$ (6 mg) was dissolved in a minimum amount of chloroform ( 200 µL) then DCPD ( 1 mL) was added. 95 µL DCPD solution, 5 µL of 1.5 %(w/w) first-generation Grubbs catalyst in chloroform, and 1 mL water solution were mixed by sonicator for 2 minutes. Then, the water phase was washed with fresh water. After 4 h, the inner phase was completely polymerized (Figure 4.27.). The solutions were drop-cast onto an aluminium surface and dried for 24 h under ambient conditions for SEM.

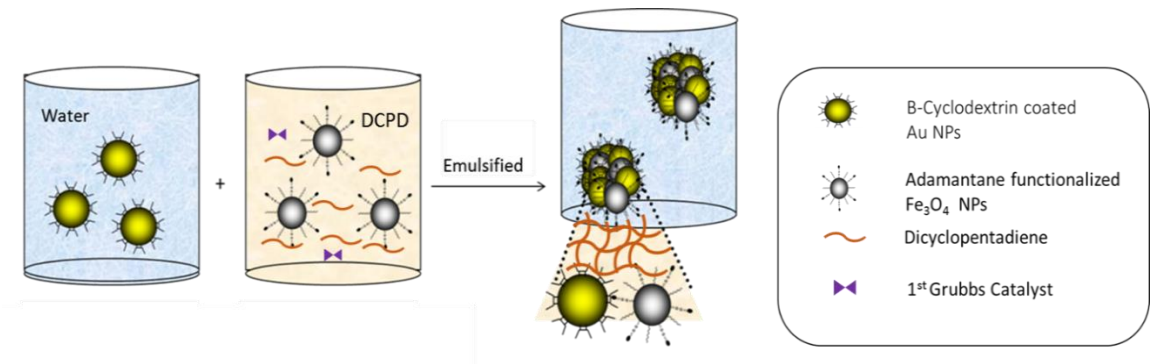


Figure 4.27. Schematic illustration of formation microcapsules.

After the inner phase of the microcapsules was polymerized, they were visualized under an optical microscope. Their sizes were observed to be around 20 μm (Figure 4.28a). These microcapsules were dried for 24 h and visualized under SEM (Figure 4.28b). It was observed that most of the microcapsules kept their spherical shape.

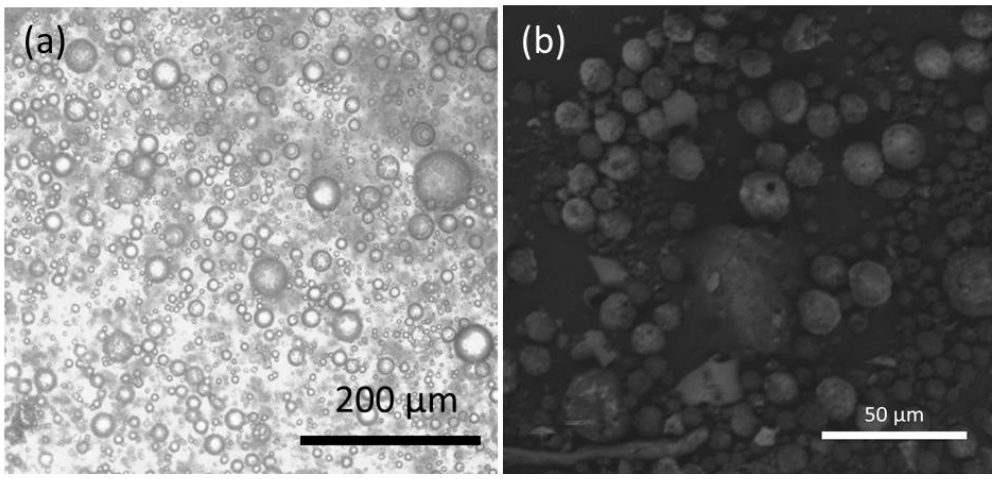


Figure 4.28. The image of microcapsules under optical microscope.

# 5. Conclusion

Stable microcapsules were fabricated by using non-covalent crosslinking of host and guest molecules at the liquid-liquid interface. As a host molecule, β-cyclodextrin coated gold nanoparticles and as a guest molecule, bis-adamantane containing linker molecules (AD-N-O-N-AD and AD-N-SS-N-AD) and adamantane functionalized iron oxide nanoparticles (AD-SS-$Fe_3O_4$ and AD-$Fe_3O_4$) were synthesized. Guest molecules containing disulfide linkage (AD-N-SS-N-AD and AD-SS- $Fe_3O_4$), microcapsules that contain those guest groups were sensitive towards reducing agent such as DTT, which means that they were disrupted after exposing to DTT. In the first part, stable microcapsules were fabricated by using β-cyclodextrin coated gold nanoparticles and bis-adamantane containing linker molecules (AD-N-O-N-AD and AD-N-SS-N-AD). They were visualized under optical microscope. Then, the Nile red dye was successfully encapsulated into the microcapsules, which were visualized under fluorescence microscope. This indicates that thus fabricated microcapsules are suitable for carrying hydrophobic molecules. After that, microcapsules contain redox-responsive guest molecules (AD-N-SS-N-AD) were exposed to DTT and release of Nile red dye from those microcapsules were observed. However, microcapsules containing non-redox responsive guest molecules (AD-N-O-N-AD) was not affected from DTT and remained stable in solution, which demonstrates that controlled hydrophobic molecule release can be accomplished by using these redox responsive microcapsules.

In the second part, adamantane functionalized iron oxide nanoparticles were used as a guest molecule in order to enable the fabricated microcapsules to have magnetic properties. Stable microcapsules were obtained by using β-cyclodextrin coated gold nanoparticles and adamantane functionalized iron oxide nanoparticles (AD-SS-$Fe_3O_4$ or AD-$Fe_3O_4$). Nile red dye was successfully encapsulated into these microcapsules and only the microcapsules which contain redox responsive adamantane functionalized iron oxide nanoparticles (AD-SS-$Fe_3O_4$) were disrupted when exposed to DTT. In contrast, microcapsules contain non-redox responsive adamantane functionalized iron oxide nanoparticles (AD- $Fe_3O_4$) stay stable even after their exposure to DTT. Hence, those microcapsules can be also used for carrying hydrophobic molecules and their release can be controlled by reducing agents in

the environment. Besides, positions of the microcapsules which contain adamantane functionalized iron oxide nanoparticles can be controlled by applying magnetic field.

As a result, in both parts, stable redox-responsive microcapsules were fabricated and their controlled dye release was displayed when they were exposed to reducing agent.

# APPENDIX A: SPECTROSCOPY DATA

$^{1}$H NMR and IR spectroscopy of the synthesized products are included. Necessary expansions were made on the NMR data.

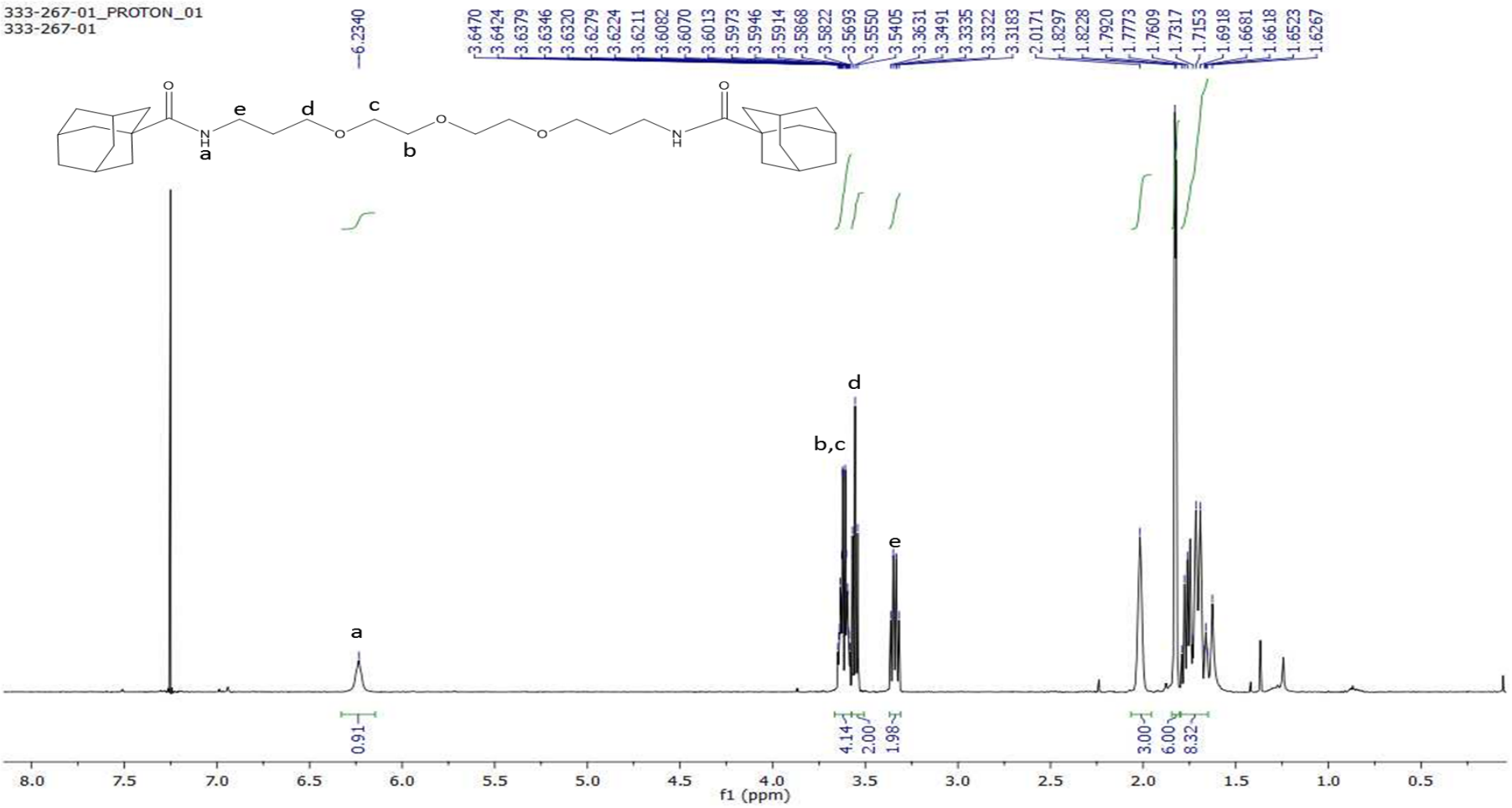


Figure A.1. $^{1}$H NMR spectrum of AD-N-O-N-AD linker molecule.

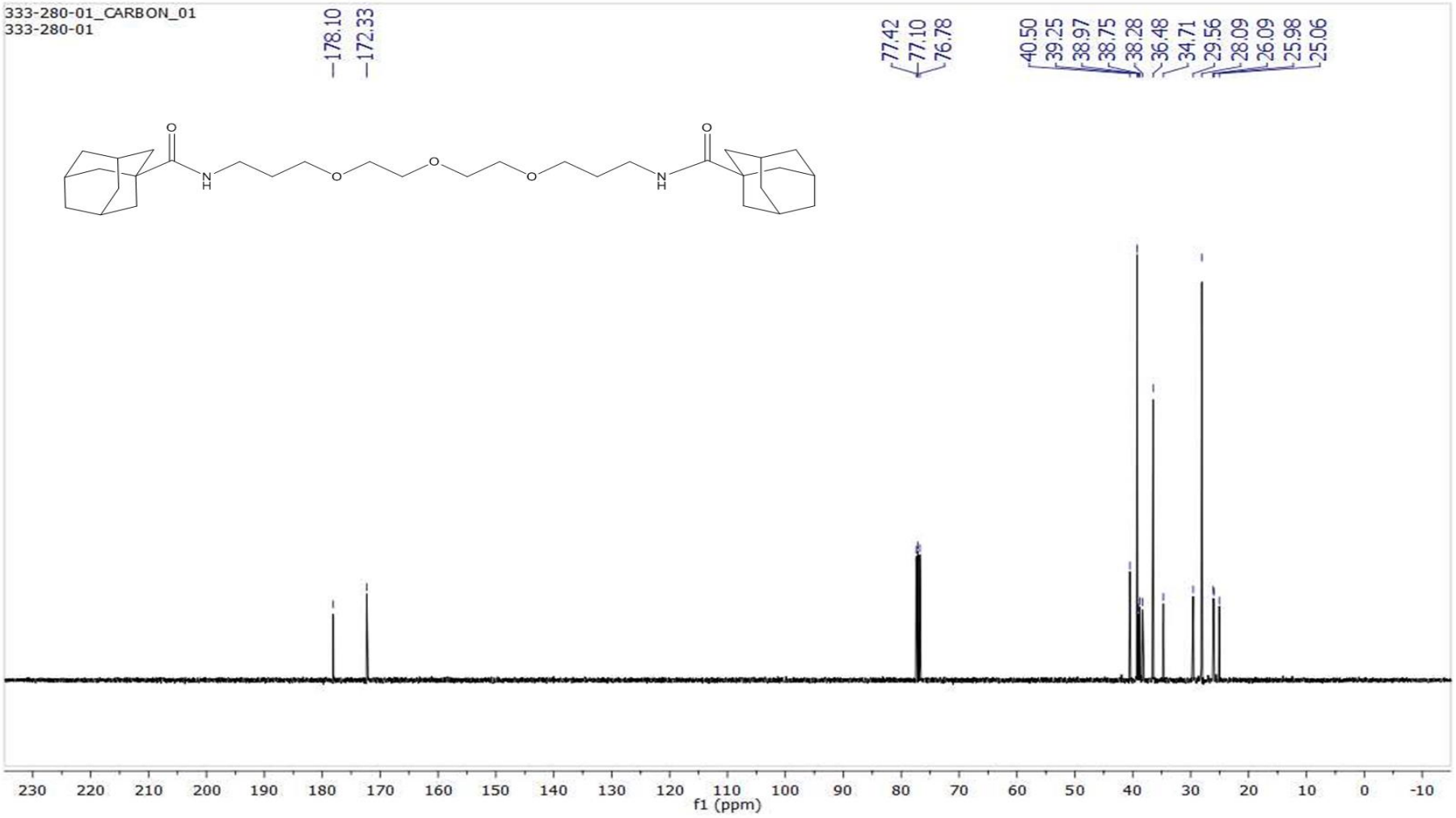


Figure A.2. $^{13}$C NMR spectrum of AD-N-O-N-AD linker molecule.

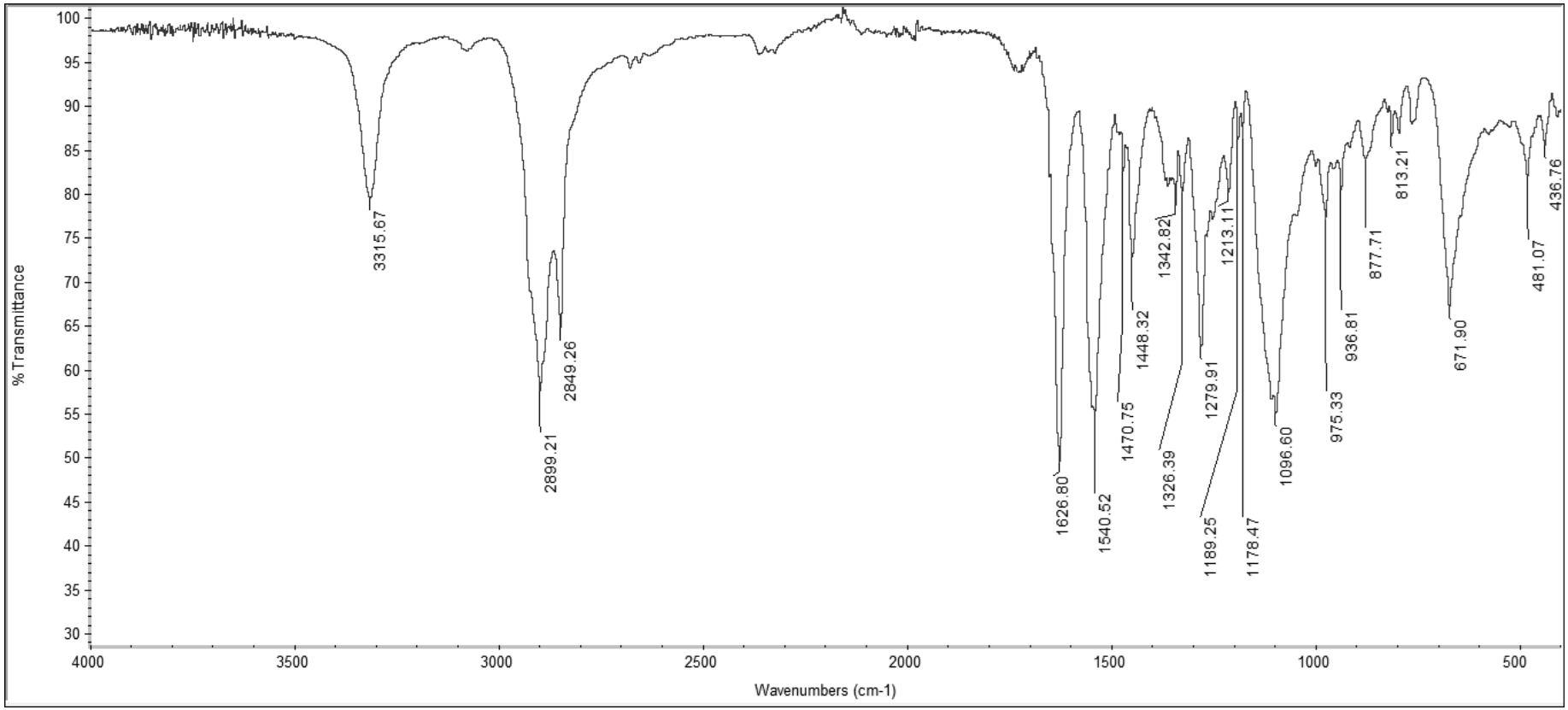


Figure A.3. FTIR spectrum of AD-SS-$CO_2$ linker molecule.

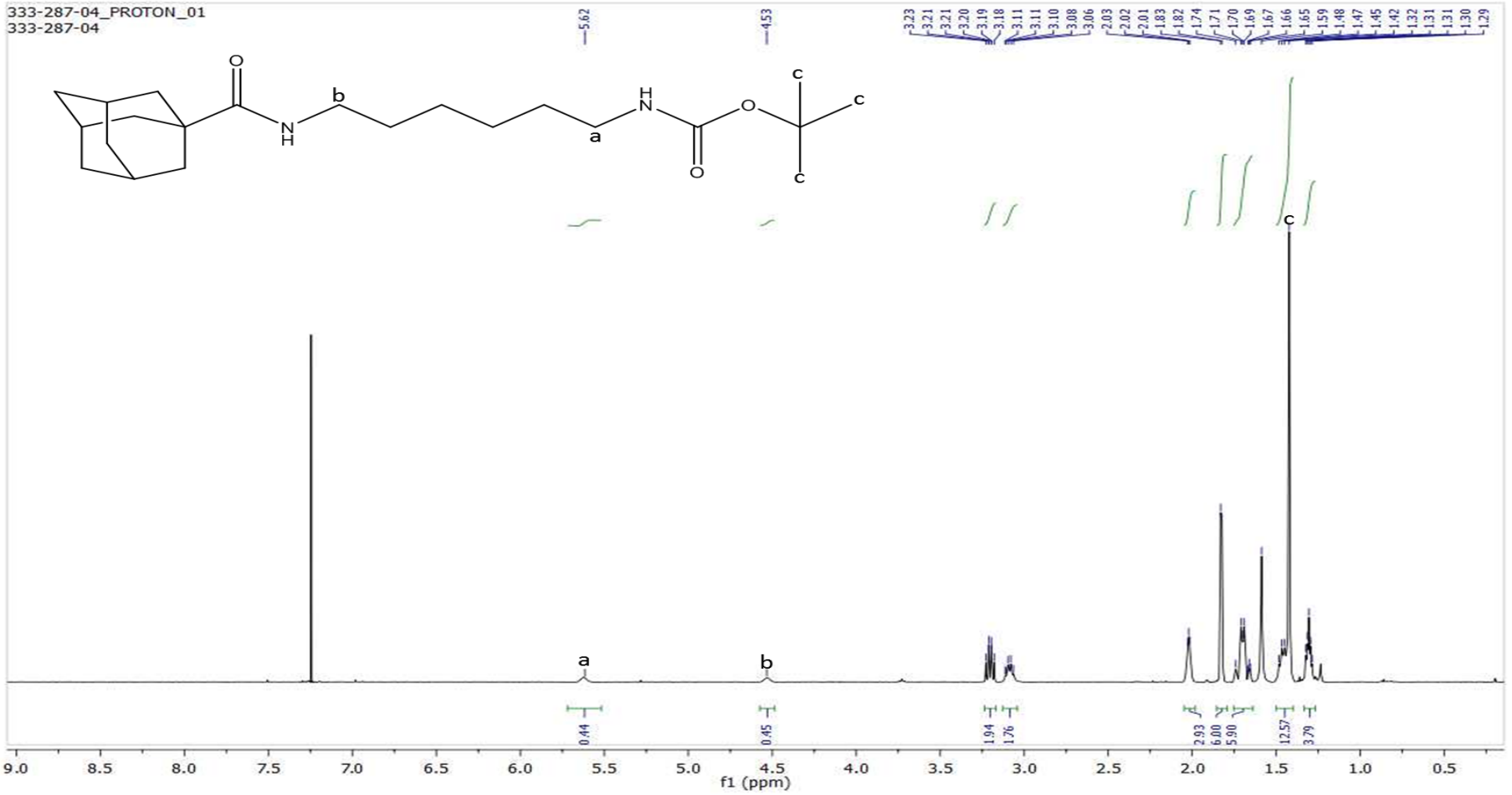


Figure A.4. $^{1}$H NMR spectrum of AD-N-Boc linker molecule.

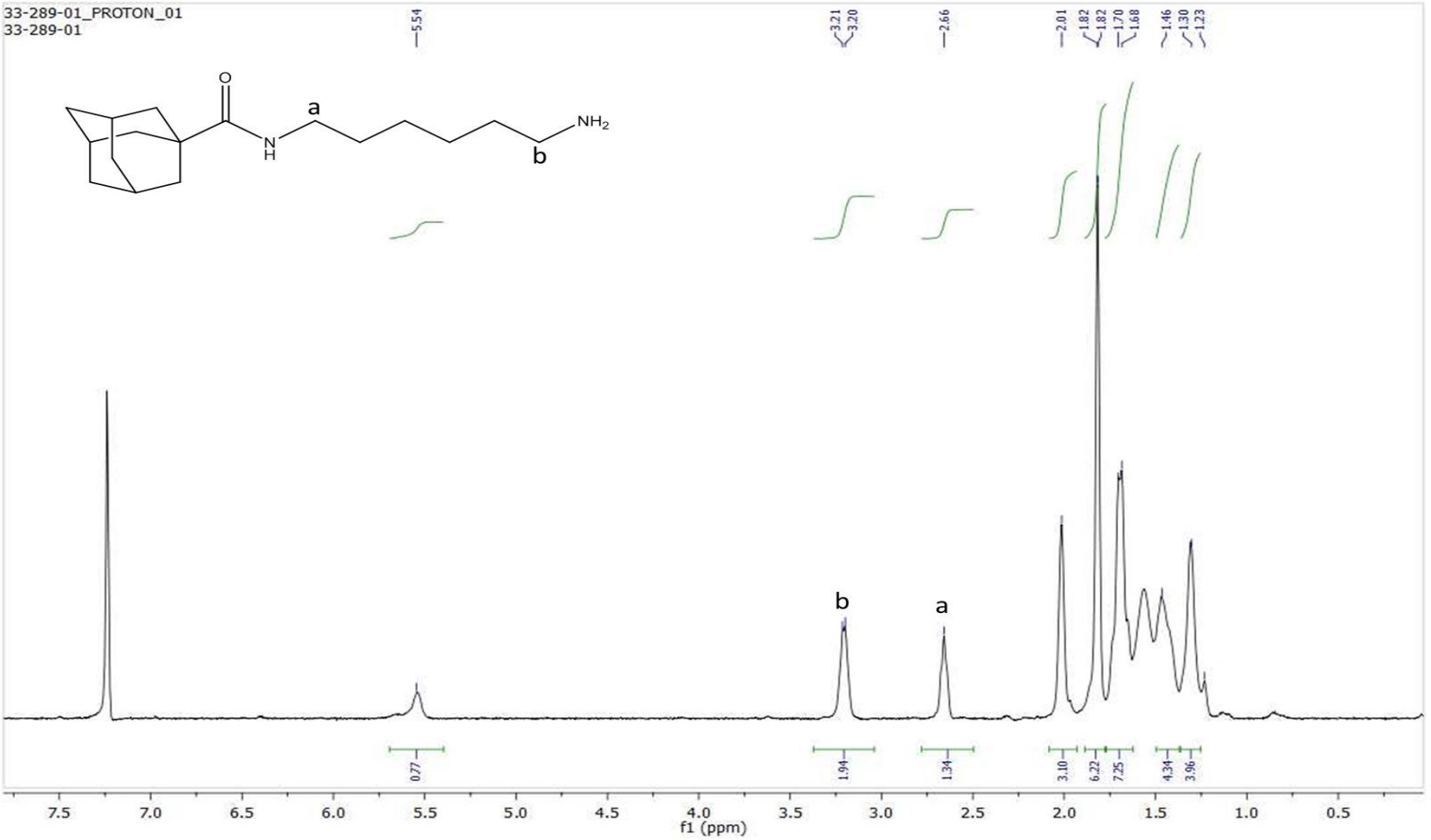


Figure A.5. $^{1}$H NMR spectrum of AD-N-Boc linker molecule.

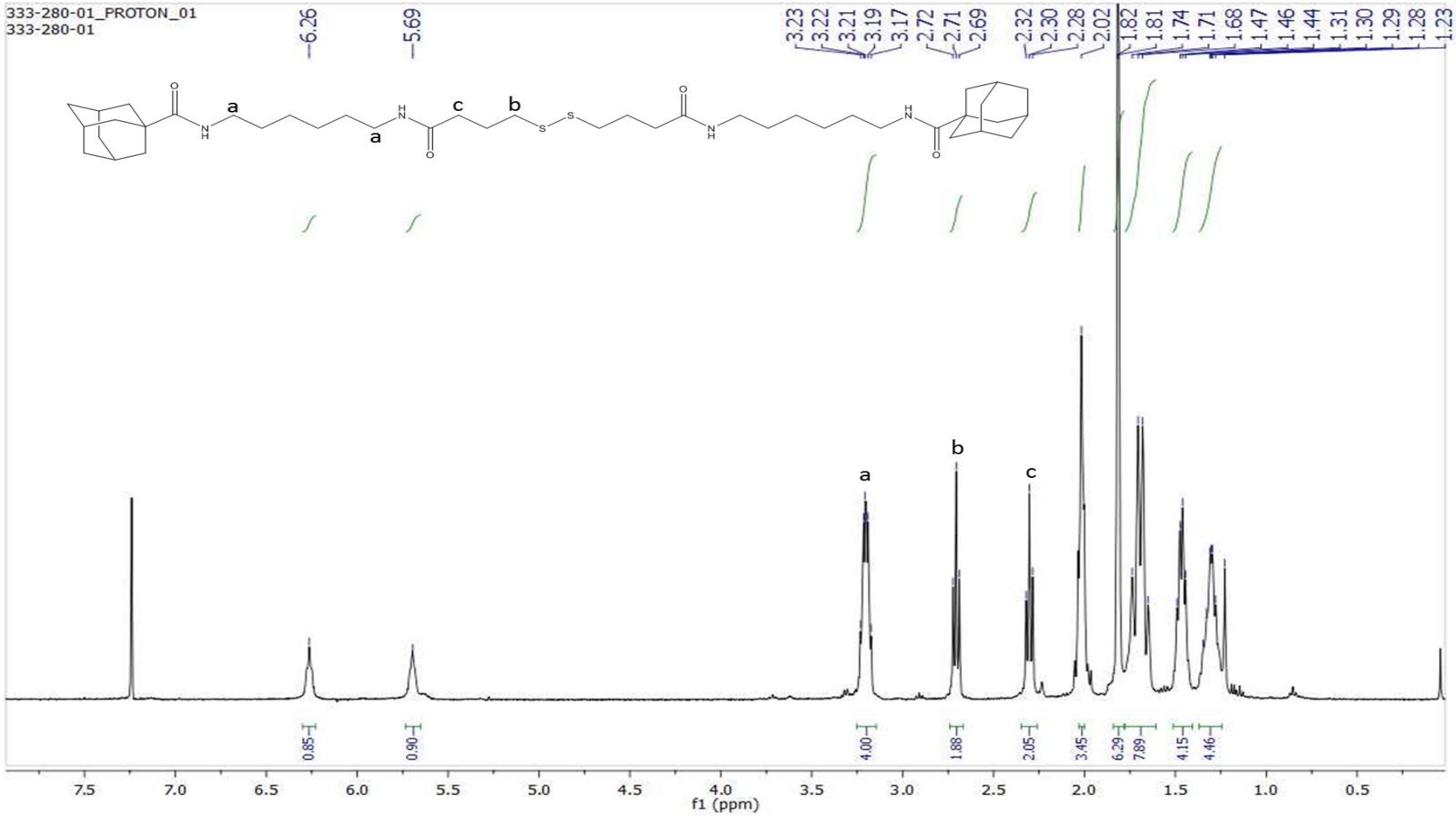


Figure A.6. $^{1}$H NMR spectrum of AD-N-SS-N-AD linker molecule.

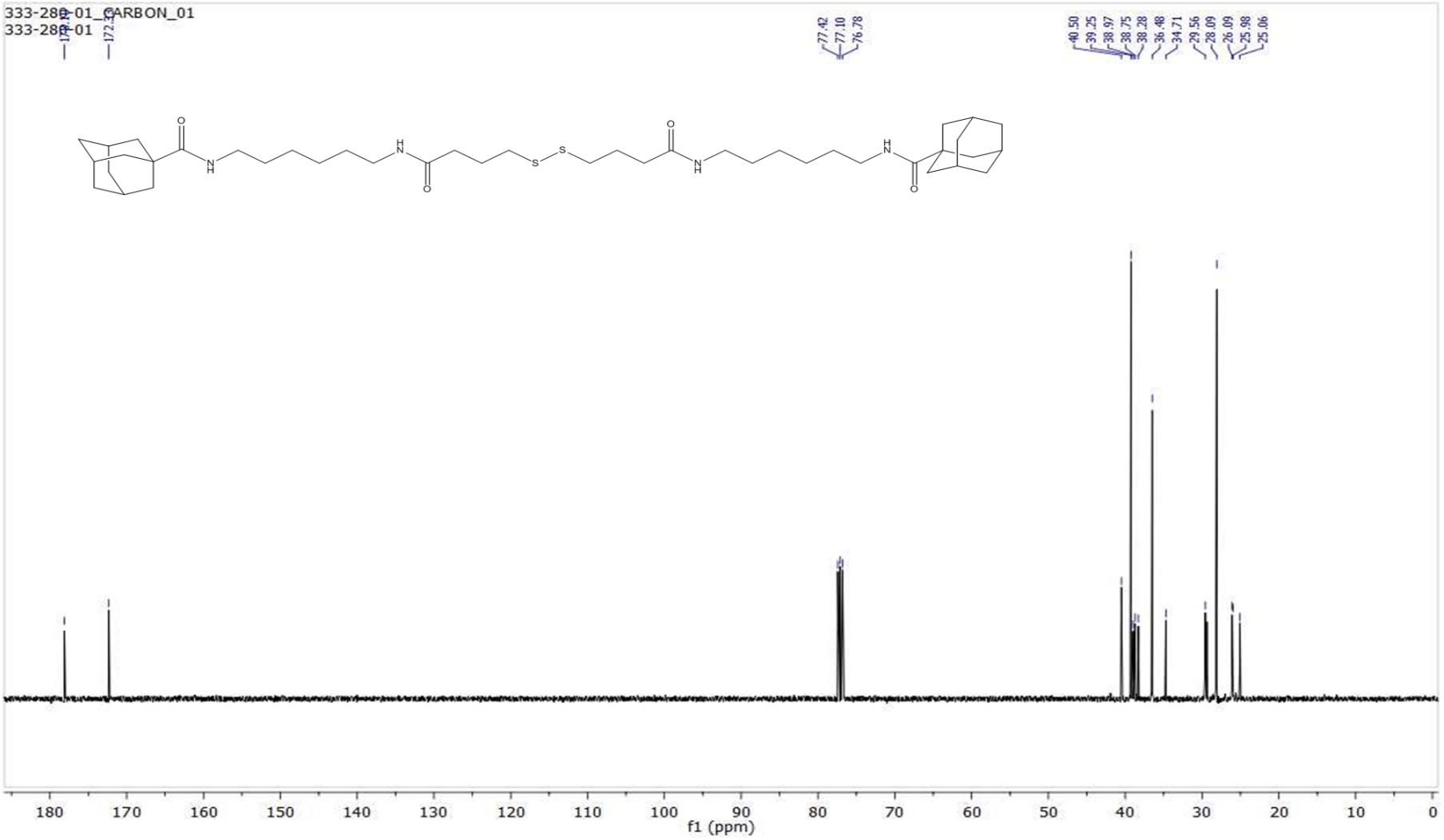


Figure A.7. $^{1}$H NMR spectrum of AD-N-SS-N-AD linker molecule.

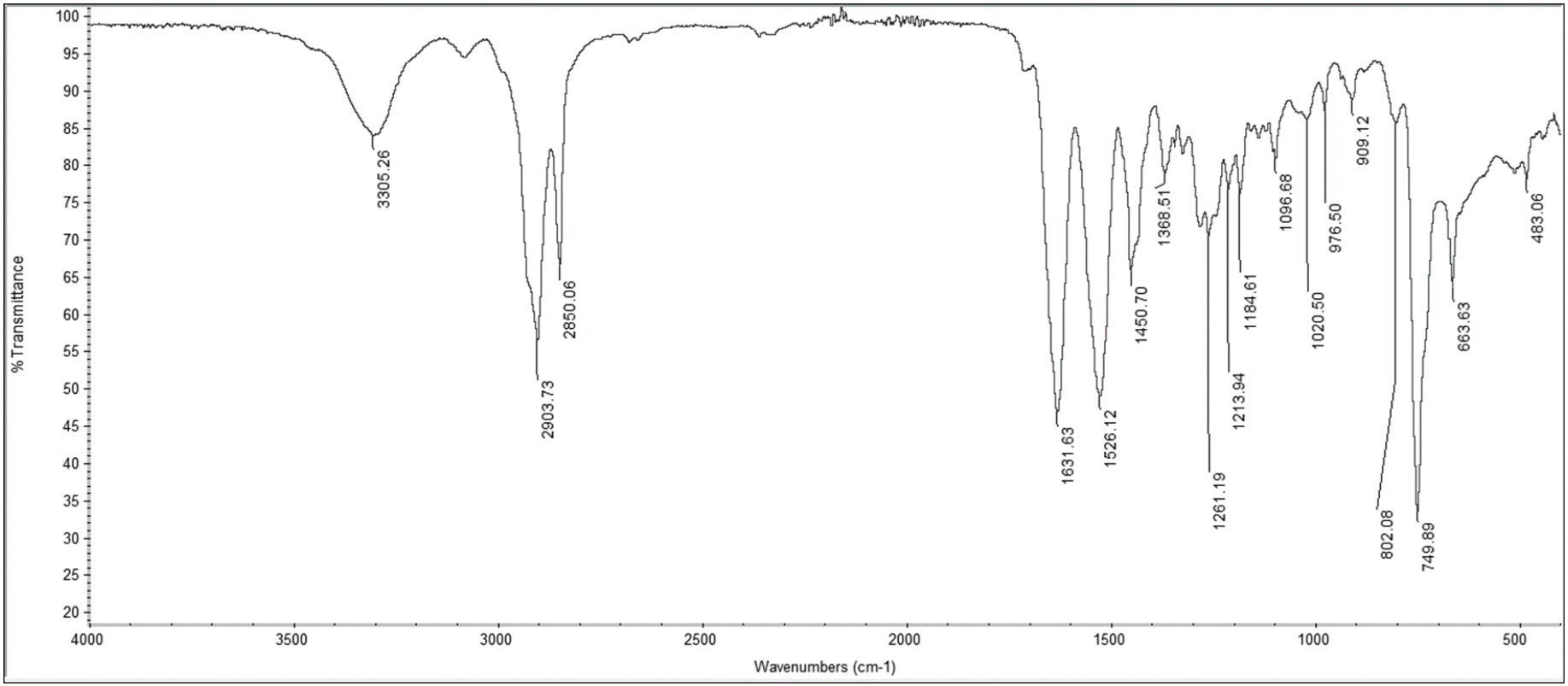


Figure A.8. FTIR spectrum of AD-N-SS-N-AD linker molecule.

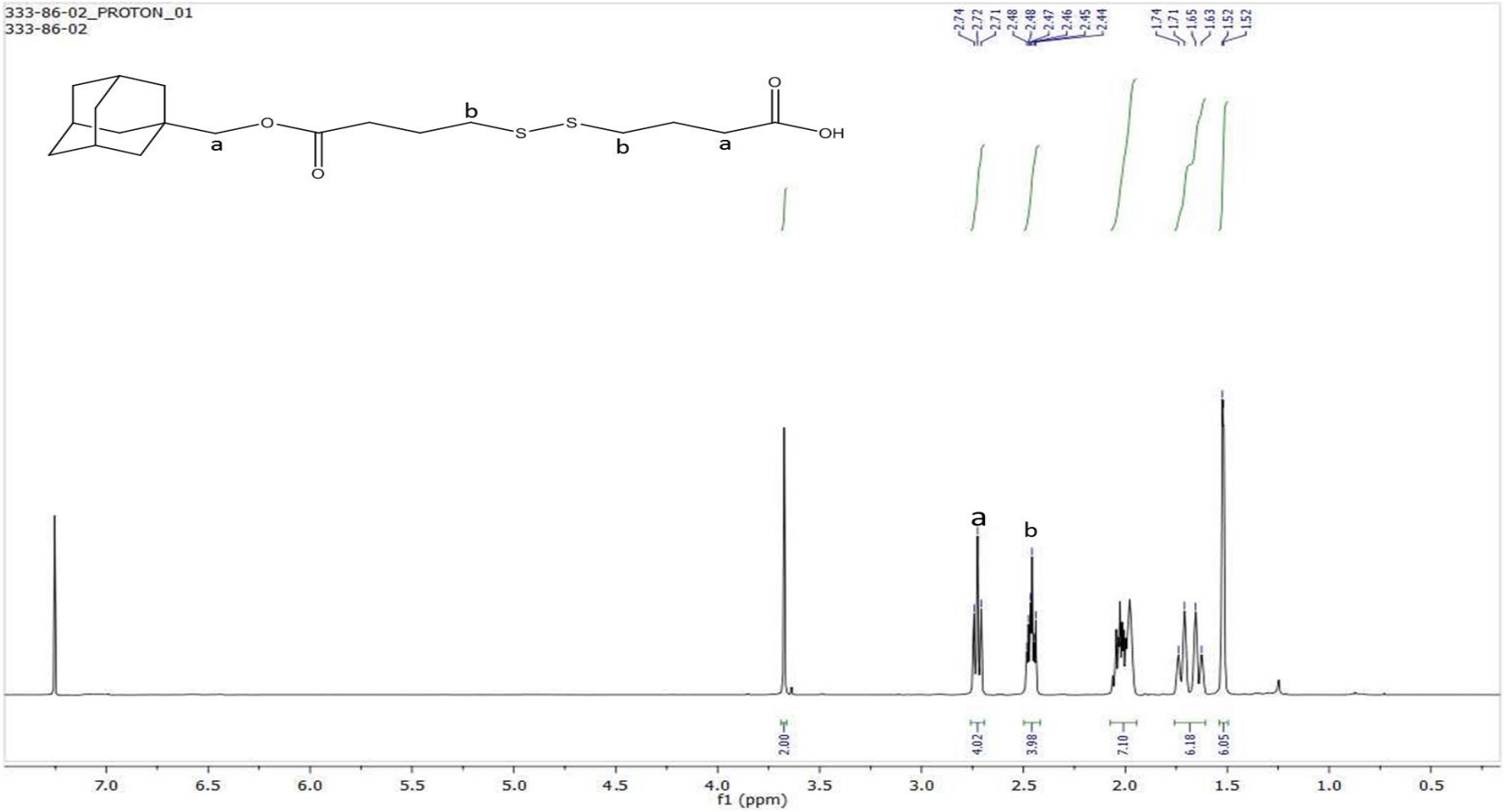


Figure A.9. $^{1}H$ NMR spectrum of AD-SS-$CO_2H$ linker molecule.

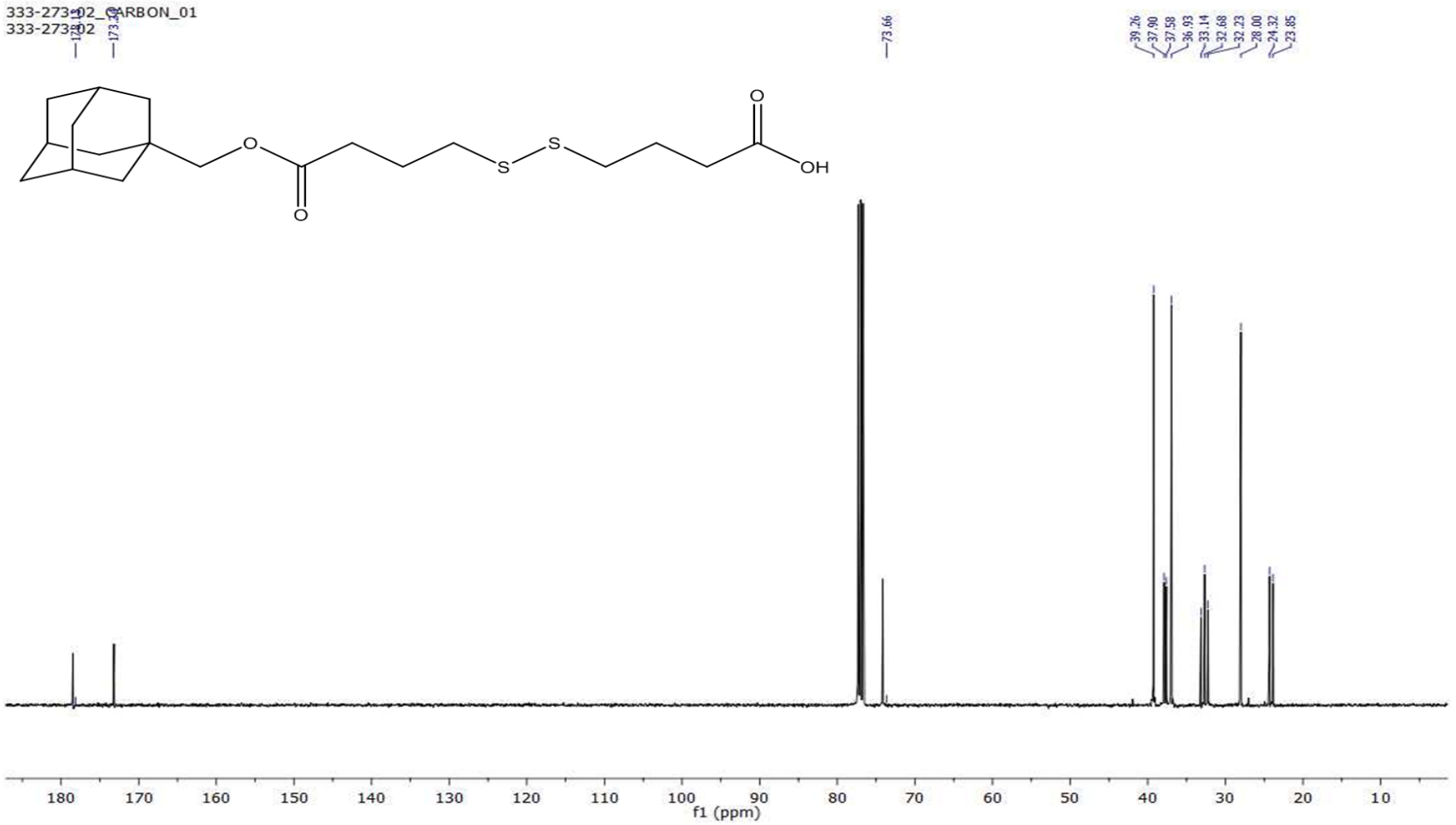


Figure A.10. $^{1}$C NMR spectrum of AD-SS-$CO_2$H linker molecule.

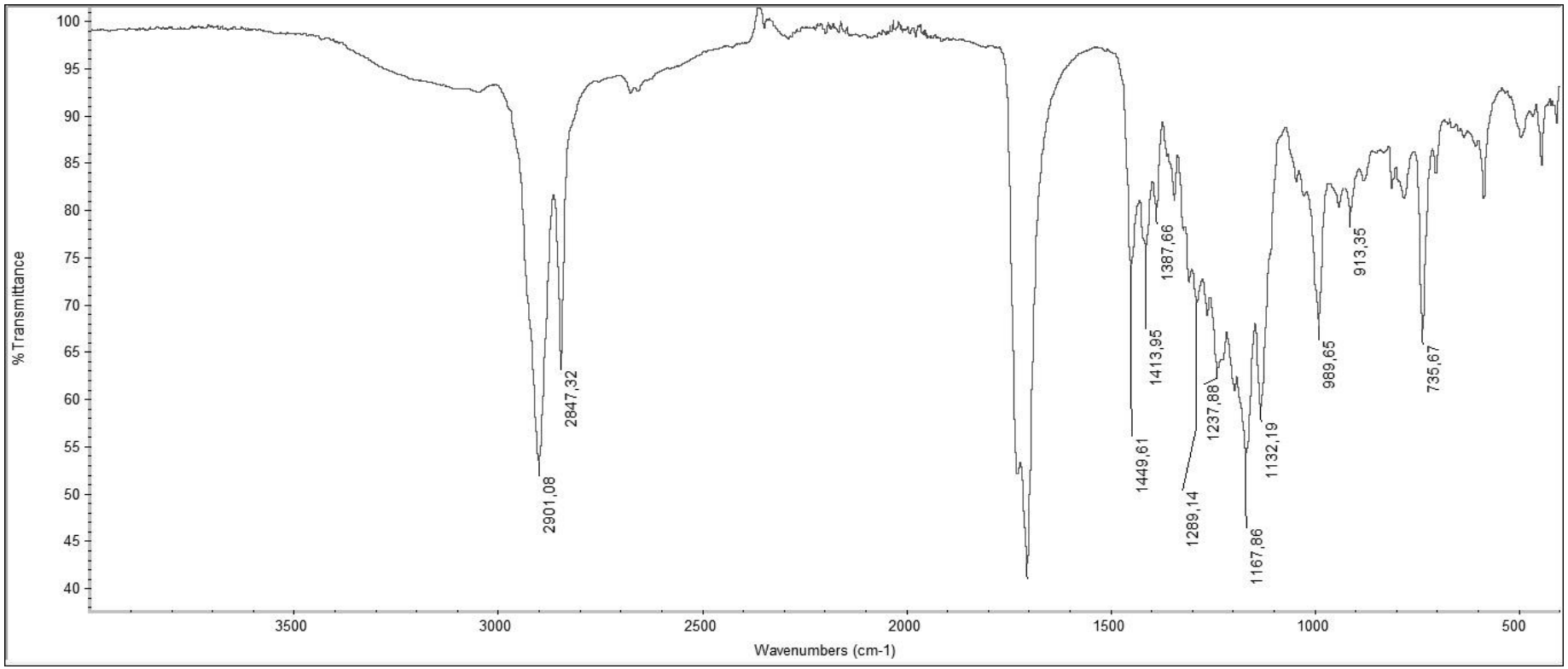


Figure A.11. FTIR spectrum of AD-SS-$CO_2H$ linker molecule.

# REFERENCES


1. Lehn, J.M., “Supramolecular Chemistry.”, *Science*, Vol. 260, pp. 1762–1763, 1993.

2. Steed, J.W., and J.L. Atwood, *Supramolecular Chemistry*, 2nd Edition, Wiley, Chichester, 2009.

3. Frieden, E., “Non-Covalent Interactions: Key To Biological Flexibility And Specificity.”, *Journal of Chemical Education*, Vol. 52, pp. 754–761, 1975.

4. Ariga, K., J.P. Hill, M. V Lee, A. Vinu, R. Charvet, and S. Acharya, “Challenges And Breakthroughs In Recent Research On Self-assembly.”, *Science and Technology of Advanced Materials*, Vol. 9, pp. 014109, 2008.

5. Lehn, J.M., “Perspectives In Supramolecular Chemistry - From Molecular Recognition Towards Molecular Information Processing And Self-organization.”, *Angewandte Chemie - International Edition in English*, Vol. 29, pp. 1304–1319, 1990.

6. Szejtli, J., “Introduction And General Overview Of Cyclodextrin Chemistry.”, *Chemical Reviews*, Vol. 98, pp. 1743–1753, 1998.

7. Connors, K. , “The Stability Of Cyclodextrin Complexes In Solution.”, *Chemical Reviews*, Vol. 97, pp. 1325–1357, 1997.

8. Granadero, D., J. Bordello, M.J. Pérez-Alvite, M. Novo, and W. Al-Soufi, “Host-guest Complexation Studied By Fluorescence Correlation Spectroscopy: Adamantane-cyclodextrin Inclusion.”, *International Journal of Molecular Sciences*, Vol. 11, pp. 173–188, 2010.

9. Dinsmore, D., M.F. Hsu, M.G. Nikolaides, M. Marquez, R. Bausch, and D. Weitz, “Colloidosomes: Selectively Permeable Capsules Composed Of Colloidal Particles.”, *Science*, Vol. 298, pp. 1006–1009, 2002.

10. Sukhorukov, G.B., A.L. Rogach, M. Garstka, S. Springer, W.J. Parak, A. Muñoz-Javier, O. Kreft, A.G. Skirtach, A.S. Susha, Y. Ramaye, R. Palankar, and M. Winterhalter, "Multifunctionalized Polymer Microcapsules: Novel Tools For Biological And Pharmacological Applications.", *Small*, Vol. 3, pp. 944–955, 2007.

11. Torchilin, V.P., "Targeted Pharmaceutical Nanocarriers For Cancer Therapy And Imaging.", *Journal of the American Association of Pharmaceutical Scientists*, Vol. 9, pp. 128–147, 2007.

12. Cavalieri, F., A. Postma, L. Lee, and F. Caruso, "Assembly And Functionalization Of DNA and Polymer Microcapsules.", *ACS Nano*, Vol. 3, pp. 234–240, 2009.

13. Peyratout, C.S., and L. Dähne, "Tailor-made Polyelectrolyte Microcapsules: From Multilayers To Smart Containers.", *Angewandte Chemie - International Edition*, Vol. 43, pp. 3762–3783, 2004.

14. Symon, Z., A. Peyser, D. Tzemach, O. Lyass, E. Sucher, E. Shezen, and A. Gabizon, "Selective Delivery Of Doxorubicin To Patients With Breast Carcinoma Metastases By Stealth Liposomes.", *Cancer*, Vol. 86, pp. 72–78, 1999.

15. Patra, D., F. Ozdemir, O.R. Miranda, B. Samanta, A. Sanyal, and V.M. Rotello, "Formation And Size Tuning Of Colloidal Microcapsules Via Host-guest Molecular Recognition At The Liquid-liquid Interface.", *Langmuir*, Vol. 25, pp. 13852–13854, 2009.

16. Binder, W.H., "Supramolecular Assembly Of Nanoparticles At Liquid-liquid Interfaces.", *Angewandte Chemie - International Edition*, Vol. 44, pp. 5172–5175, 2005.

17. Chandra, P., J. Singh, A. Singh, A. Srivastava, R.N. Goyal, and Y.B. Shim, "Gold Nanoparticles And Nanocomposites In Clinical Diagnostics Using Electrochemical Methods.", *Journal of Nanoparticles*, Vol. 2013, 2013.

18. Ali, M.E., U. Hashim, S. Mustafa, Y.B. Che Man, and K.N. Islam, "Gold Nanoparticle Sensor For The Visual Detection Of Pork Adulteration In Meatball Formulation.", *Journal of Nanomaterials*, Vol. 2012, 2012.

19. Stuchinskaya, T., M. Moreno, M.J. Cook, D.R. Edwards, and D. Russell, “Targeted Photodynamic Therapy Of Breast Cancer Cells Using Antibody-phthalocyanine-gold Nanoparticle Conjugates.”, *Photochemical & Photobiological Sciences,* Vol. 10, pp. 822–831, 2011.

20. Brown, S.D., P. Nativo, J.A. Smith, D. Stirling, P.R. Edwards, B. Venugopal, D.J. Flint, J. a. Plumb, D. Graham, and N.J. Wheate, “Gold Nanoparticles For The Improved Anticancer Drug Delivery Of The Active Component Of Oxaliplatin.”, *Journal of the American Chemical Society*, Vol. 132, pp. 4678–4684, 2010.

21. Turkevich, J., P.C. Stevenson, and J. Hillier, “A Study Of The Nucleation And Growth Processes In The Synthesis Of Colloidal Gold.”, *Discussions of the Faraday Society*, Vol. 11, pp. 55–75, 1951.

22. Brust, M., M. Walker, D. Bethell, D.J. Schiffrin, and R. Whyman, “Synthesis Of Thiol-derivatised Gold Nanoparticles In.”, *Journal of the Chemical Society*, Vol. 32, pp. 801–802, 2000.

23. Verma, A., and V.M. Rotello, “Surface Recognition Of Biomacromolecules Using Nanoparticle Receptors.”, *Chemical Communications* , Vol. 3, pp. 303–312, 2005.

24. Krasovskii, V.I., V. Karavanskii, N. Orlov, I. Nagovitsyn, V. V. Savranskii, and G.K. Chudinova, “Surface Plasmon Resonance In Protein Covered Gold Nanoparticles.”, *Solid State Physics*, Vol. 6606, pp. 305-306, 2007.

25. Huang, X., and M. El-Sayed, “Gold Nanoparticles: Optical Properties And Implementations In Cancer Diagnosis And Photothermal Therapy.”, *Journal of Advanced Research*, Vol. 1, pp. 13–28, 2010.

26. Yallapu, M.M., S.F. Othman, E.T. Curtis, B.K. Gupta, M. Jaggi, and S.C. Chauhan, “Multi-functional Magnetic Nanoparticles For Magnetic Resonance Imaging And Cancer Therapy.”, *Biomaterials*, Vol. 32, pp. 1890–1905, 2011.

27. Liong, M., J. Lu, M. Kovochich, T. Xia, S.G. Ruehm, A.E. Nel, F. Tamanoi, and J.I. Zink, “Multifunctional Inorganic Nanoparticles For Imaging, Targeting, And Drug Delivery.”, *ACS Nano*, Vol. 2, pp. 889–896, 2008.

28. Laurent, S., D. Forge, M. Port, A. Roch, C. Robic, L. Vander Elst, and R.N. Muller, "Magnetic Iron Oxide Nanoparticles: Synthesis, Stabilization, Vectorization, Physicochemical Characterizations And Biological Applications.", *Chemical Reviews*, Vol. 108, pp. 2064–2110, 2008.

29. Lin, P.C., C.C. Yu, H.T. Wu, Y.W. Lu, C.L. Han, A.K. Su, Y.J. Chen, and C.C. Lin, "A Chemically Functionalized Magnetic Nanoplatform For Rapid And Specific Biomolecular Recognition And Separation.", *Biomacromolecules*, Vol. 14, pp. 160–168, 2013.

30. Wu, W., Q. He, and C. Jiang, "Magnetic Iron Oxide Nanoparticles: Synthesis And Surface Functionalization Strategies.", *Nanoscale Research Letters*, Vol. 3, pp. 397–415, 2008.

31. Ramsden, W., "Separation Of Solids In The Surface-layers Of Solutions And Suspensions.", *Proceedings of the Royal Society of London*, Vol. 72, pp. 156, 1903.

32. Pickering, S.U., "Emulsions.", *Journal of the Chemical Society*, Vol. 91, pp. 2001–2021, 1907.

33. Velev, O.D., K. Furusawa, and K. Nagayama, "Assembly Of Latex Particles By Using Emulsion Droplets As Templates .2. Ball-like And Composite Aggregates.", *Langmuir*, Vol. 12, pp. 2385–2391, 1996.

34. Hsu, M.F., M.G. Nikolaides, A.D. Dinsmore, A.R. Bausch, V.D. Gordon, X. Chen, J.W. Hutchinson, D. A. Weitz, and M. Marquez, "Self-assembled Shells Composed Of Colloidal Particles: Fabrication And Characterization.", *Langmuir*, Vol. 21, pp. 2963–2970, 2005.

35. Kim, J. W., A. Fernández-Nieves, N. Dan, A.S. Utada, M. Marquez, and D. A. Weitz, "Colloidal Assembly Route For Responsive Colloidosomes With Tunable Permeability.", *Nano Letters*, Vol. 7, pp. 2876–2880, 2007.

36. Bon, S. A. F., S. Cauvin, and P.J. Colver, "Colloidosomes As Micron-sized Polymerisation Vessels To Create Supracolloidal Interpenetrating Polymer Network Reinforced Capsules.", *Soft Matter*, Vol. 3, pp. 194–199, 2007.

37. Bon, S. F., and T. Chen, “Pickering Stabilization As A Tool In The Fabrication Of Complex Nanopatterned Silica Microcapsules.”, *Langmuir*, Vol. 23, pp. 9527–9530, 2007.

38. Chen, T., P.J. Colver, and S. A. F. Bon, “Organic-inorganic Hybrid Hollow Spberes Prepared From TiO2-stabilized Pickering Emulsion Polymerization.”, *Advanced Materials*, Vol. 19, pp. 2286–2289, 2007.

39. Binks, B.P., “Particles As Surfactants—similarities And Differences.”, *Current Opinion in Colloid & Interface Science*, Vol. 7, pp. 21–41, 2002.

40. Salari, J., *Pickering Emulsions, Colloidosomes & Micro-Encapsulation.*, Eindhoven University of Technology Press , Eindhoven, 2011.

41. Atkins, P., and J. D. Paula, *Physical Chemistry*, 8th Edition, Oxford University Press, New York, 2006.

42. Samanta, B., D. Patra, C. Subramani, Y. Ofir, G. Yesilbag, A. Sanyal, and V.M. Rotello, “Stable Magnetic Colloidosomes Via Click-mediated Crosslinking Of Nanoparticles At Water-oil Interfaces.”, *Small*, Vol. 5, pp. 685–688, 2009.

43. Ali, M., S. Bora, and S.K. Ghosh, “Composite-Walled Magnetic Microcapsules At The Water-Toluene Interface By Ligand Polymerization.”, *Langmuir*, Vol. 30, pp. 10449–10455, 2014.

44. Jeong, Y., Y.C. Chen, M.K. Turksoy, S. Rana, G.Y. Tonga, B. Creran, A. Sanyal, A.J. Crosby, and V.M. Rotello, “Tunable Elastic Modulus Of Nanoparticle Monolayer Films By Host-guest Chemistry.”, *Advanced Materials*, Vol. 26, pp. 5056–5061, 2014.

45. Saito, G., J. Swanson, and K.D. Lee, “Drug Delivery Strategy Utilizing Conjugation Via Reversible Disulfide Linkages: Role And Site Of Cellular Reducing Activities.”, *Advanced Drug Delivery Reviews*, Vol. 55, pp. 199–215, 2003.

46. Son, S., R. Namgung, J. Kim, K. Singha, and W.J. Kim, “Bioreducible Polymers For Gene Silencing And Delivery.”, *Accounts of Chemical Research*, Vol. 45, pp. 1100–1112, 2012.

47. Mitchell, J.B., and A. Russo, “The Role Of Glutathione In Radiation And Drug Induced Cytotoxicity.”, *The British Journal of Cancer* , Vol. 8, pp. 96–104, 1987.

48. Ashton, P.R., R. Koniger, J.F. Stoddart, D. Alker, and V.D. Harding, “Amino Acid Derivatives Of Beta-cyclodextrin.”, *Journal of Organic Chemistry*, Vol. 61, pp. 903–908, 1996.

49. Dernaika, H., S. V Chong, C.G. Artur, and J.L. Tallon, “Spectroscopic Identification Of Neurotoxin Tetramethylenedisulfotetramine ( TETS ) Captured By Supramolecular Receptor $\beta$ -Cyclodextrin Immobilized On Nanostructured Gold Surfaces.”, *Journal of Nanomaterials*, Vol. 2014, 2014.

50. Liu, F. K., “Using Size-Exclusion Chromatography To Monitor Variations In The Sizes Of Microwave-Irradiated Gold Nanoparticles.”, *ISRN Chromatography*, Vol. 2012, pp. 1–7, 2012.

51. Shendage, D.M., and R. Fro, “Highly Efficient Stereoconservative Amidation And Deamidation Of R -Amino Acids.”, *Journal of the American Chemical Society*, Vol. 135, pp. 1986–1989, 2004.

52. Park, J., K. An, Y. Hwang, J. Park, J.I.N. Noh, J. E.Y. Kim, J. Park, and N. Hwang, “Ultra-large Scale Syntheses Of Monodisperse Nanocrystals Via A Simple And Inexpensive Route.”, *Nature*, Vol. 3, pp. 1–13, 2004.